

The authors would like to thank Alexei Lyapustin for his feedback. As a result, we have made some changes to the structure of the manuscript.

This paper describes an updated MISR research algorithm for aerosol and chlorophyll retrieval over Case 1 waters. The improvements include a standard explicit model of underlight as a function of Chl, and, importantly, improvements in calibration, including new de-trending analysis particularly important for climate research applications. This is a solid work that needs to be published with minor revision.

General comment: While generally the paper is written reasonably well, an improvement in structure/logic would be very helpful. Currently, the text unfolds almost unstructured as a story: the details of algorithm are mixed with calibration, past and new work, and at some point it becomes rather confusing as to what new is specifically done here.

It could help if you could structure these things upfront in Introduction.

We have restructured the paper such that we believe it now flows more clearly.

Page 2, lines 31-32: Ocean reflectance in the blue can be higher than 5-20%; as far as I know, Gordon referred to Red band with respect to relative contribution.

Blue albedo in case I waters appears to peak at about 20% according to Figure 2 from our paper. The 5-20% is from our work here, and might be specific to the MISR channels.

Page 3, lines 21-22: Be more specific: which model is used - is it isotropic Cox-Munk, or Nakajima-Tanaka, or something else?

We have made it clear in the text that the model is isotropic Cox-Munk.

Page 3, line 28: How is the MISR Standard product surface pressure aliased from nearby mountains to over ocean?

As a single surface pressure value is used for a 17.6 km region, and we do retrievals at 1.1 km resolution, it is possible for errors to manifest themselves as we approach the coast (if there are mountains nearby).

Page 3, line 29: To use all 4 bands, you need to accurately limit to Case-1 waters. How is it done?

The χ^2 parameter (calculated over all 4 wavelengths) and our χ^2_{Chl} parameter should be effective at limiting results to only case I. Because the Chl parameterization is based on a case I framework, our model-measurement fits

should be very poor in case II conditions; this is true for the cases we've tried. This is now mentioned in the text.

Page 8, line 28: Lyapustin et al. technique does full atmospheric correction of MODIS TOA data, contrary to this approach, as described. Thus, the core assumption that the AOD is assumed temporally stable, should be explicitly mentioned.

We agree, and have added that the AOD is assumed to be temporally stable.

Page 12, line 7: To give reader a good reference frame for MISR data, can you provide the same numbers for the SeaWIFS - Terra comparison (these are widely available).

We could provide the numbers in a table (as a Terra-SeaWIFS comparison on the SeaBASS website takes only a few seconds to compute), but they would be for a completely different sample subset, and so might not be comparable to the data presented. However, we have commented on comparisons between MODIS-Terra, SeaWIFS, and SeaBASS in the text, including mentioning that SeaWIFS agrees better with MODIS-Terra than MISR does.

Reviewer 2

The authors would like to thank reviewer 2 for their feedback. As a result, we have made some modifications to the manuscript.

One of my main problems is with how the paper is organized, and the relative weight given to describing tweaks to MISR calibration and the incorporation of Chl-a in the Research Algorithm (RA). These are two entirely separate issues, and honestly I think the audience for the latter is far larger than the former (especially considering the literature by the authors and others about calibration in the last few years). This paper feels more like a progress report of all activities performed in a period of time, which isn't the best way to present results to the community. I think this would be a far stronger paper if the calibration changes were either published elsewhere, or in an addendum or the supplementary material. At the very least, a clearer separation in the paper between topics related to calibration and the coupled Chl-a retrieval is needed.

Because of the spectrally varying nature of MISR's calibration (e.g., the green band has degraded much faster than the blue), it makes sense to address the calibration in this paper. As the reviewer is well aware, there is a high degree of correlation between ratios of blue-to-green water leaving radiance and retrieved chlorophyll-a. Therefore, any calibration (or stray-light) artifacts that affect this ratio need to be taken into account before the analysis is performed. We have included this point in the main text, and moved the calibration section into an appendix.

I'm also concerned with the methods used to validate the Chl-a coupled retrieval. Comparisons with SeaBASS are an obvious way of doing things, but of course the number of match-ups available for comparison are limited. What bothers me is the 'validation' against MODIS results. As the authors note, the multi-angle MISR data have access to more information about aerosols, while MODIS has channels better suited for Chl-a retrievals. Differences between coupled algorithm MODIS and MISR results could be due to either instrument – MODIS is not necessarily a standard to which MISR should be held. What is the value, then, of a scatterplot of MODIS and MISR Chl-a results?

We agree that this is more a comparison against MODIS than a formal validation, as we make clear in the text. However, the MODIS product is a standard for the ocean color community, and its properties have been studied by many groups. For example, the SeaBASS website gives error statistics for MODIS-Terra, which we also note in the paper. As such, comparing MISR to MODIS-Terra is useful, in part because they share the same platform, in part because MODIS Chl is a better-known and substantially validated quantity, and in part because there are vastly more MISR-MODIS coincidences than MISR-SeaBASS coincidences. Further, we note that before presenting the MISR-MODIS comparison, we present the MISR-SeaBASS comparison, for which there are only 49 points.

Continuing with a discussion coupled Chl-a retrievals, why is there no attempt to determine the uncertainty in such a result based on the components of the RA? SeaBASS data uncertainties are mentioned at one point, but why are those uncertainties are also not incorporated into any validation?

The RA is a coupled atmospheric and surface algorithm compiled into a self-consistent aerosol/Chl retrieval algorithm with appropriate spectral and angular weighting. As there is limited information on the separate uncertainty of each component, we assess the uncertainty for the coupled system. We have added error bars (for SeaBASS) to the scatter-plots.

There are a number of statistical tools available to test the hypothesis that dataset A is identical to dataset B. These simple tools go beyond comparisons of correlation coefficients, etc. and actually state the confidence intervals for agreement, taking into account things such as sample size. A problematic example is in the abstract, where it is noted that MODIS has a higher correlation coefficient (0.91) than MISR (0.86). Given the small sample size, these differences are probably statistically insignificant.

We agree that the MISR-SeaBASS comparison is unlikely to be statistically significant, and we perform a two-sample Kolmogorov-Smirnov test to indicate that the MISR-MODIS results cannot be distinguished from each other, with better than 95% certainty. We made the MISR-SeaBASS comparison for completeness, as the SeaBASS data are considered ground

truth, but we also made the MISR-MODIS comparison, as mentioned earlier, in part to address the SeaBASS-MISR sampling limitations. We have modified the abstract, validation, and conclusions to improve the paper and address these points.

Please get an statistics textbook, learn some hypothesis testing techniques, and start applying them. I've also found the following publication to be useful even if it comes from outside our discipline: Altman, D. G. & Bland, J. M. (1983). Measurement in medicine: the analysis of method comparison studies. The statistician, 307–317.

We are of course familiar with the standard hypothesis tests, such as the Student's T-test, and even with some more advanced tests that do not assume a Gaussian form for the underlying distributions. We have applied a two sample Kolmogorov-Smirnov test to assess the distinguishability of datasets in the paper. However, the statistics are still provided in Tables 1 and 2.

I also wonder why the authors never tested the new RA coupled algorithm on synthetic data. Given the limited SeaBASS dataset, doesn't at least confirming the new algorithm can successfully operate on synthetic data have merit? Presumably this is part one of a two (or more?) part series? I think how this paper fits in that series needs to be discussed.

As the MISR-SeaBASS dataset is so limited, a key part of our motivation for the MISR-MODIS comparison. As discussed above, this allows us to compare MISR to MODIS-Terra's already validated Chl. The focus of our research program in general is aerosols, so our first objective here is to improve the lower boundary condition over ocean. If a MISR-derived Chl product proves to be of value to the community despite the reduced coverage and sub-optimal spectral bands compared to MODIS, we would consider further Chl validation in a future study.

Detailed comments

Page 1, line 19-21: I fully do not understand the first sentence of this paragraph – you are running the algorithm to validate the algorithm and somehow also analyze corresponding MODIS data? I think this becomes clearer later on in the paper, but at this point this serves more to confuse than illuminate.

We agree that this is a little confusing. It has been rewritten.

Page 1, line 21-23: Does it really make sense to compare a correlation coefficient of 0.91 to 0.86, especially for a small dataset? I think a better way of saying this is that they are statistically identical which brings me again to the point that you should be using hypothesis testing.

The MISR-SeaBASS comparison is performed solely because SeaBASS is a standard used for ocean color validation. The MISR-MODIS comparison is included specifically to obtain adequate statistics; we now make it clear in the text that the MISR and MODIS data cannot be distinguished using a two-sample Kolmogorov-Smirnov test.

Page 1, line 25: it's not clear at this point the meaning of looking only at Chl<1.5

We have clarified our reasoning behind this by indicating that this is the region we expect meaningful results from our Chl model. It is also the regime where the empirical, oligotrophic water Chl algorithm used by much of the ocean color community has its best performance [e.g., Hu et al., JGR 2012].

Page 1-2, final abstract sentence: While I agree that this might be the case, I'm not sure you've demonstrated this in this paper, particularly for the value of joint MISR-MODIS retrievals.

We believe our statement is worded appropriately. We are just indicating that one of MISR's strengths is its ability to diagnose aerosol type (due to having multiple camera angles), and that a future MISR-MODIS retrieval algorithm could leverage this strength appropriately. Similarly, we note that MODIS provides superior spectral information content for this application.

Page 2, line 13: an appropriate continuation of the last sentence of this paragraph would be "assuming that ocean and aerosol signals at TOA don't co-vary."

Right, we added that.

Page 3, line 27: It would be good to give either a description or a reference for where the MISR SA wind data come from, and not assume all readers inherently know this.

You are correct, and we have added a reference to a personal communication with Mike Garay, who currently maintains the SA. Basically, the wind comes from monthly Quikscat (prior to ~2011) and SSMI (2011 onwards) wind speed data.

Page 3, line 27: Why doesn't MISR use NCEP or other modeled products for sea surface pressure? Is that what the SA does, and you're now setting this to 1013.25 because of mountains near the ocean?

Many of the decision about ancillary inputs to the SA were made more than a decade ago, when computer resources, storage, throughput, etc., were quite limited compared to today. To run the SA operationally on the entire MISR datastream at the time, the SA uses one value of monthly-modeled pressure for each 17.6 km x 17.6 km region. This can result in over-ocean errors in the

RA retrievals where the elevation changes dramatically near the coast. Given the small variations in surface sea-level pressure relative to the mean over cloud-free scenes where the over-water retrievals are performed, using 1013.25 mb as the surface pressure is reasonable.

Page 4, lines 2-4: I think separate weighting for aerosol and ocean components of a retrieval would be difficult to implement practically, as the appropriate weights are most likely scene dependent.

In general, the weighting for the ocean surface component could be μ , whereas the aerosol component could be μ^{-1} . This makes use of the greater surface contribution to the TOA reflectance, relative to the atmospheric contribution, in the near-nadir cameras, and conversely, the greater atmospheric contribution to the steeper-angle signals. However, as we have not implemented this aerosol/ocean weighting algorithm yet (as was noted in the text), we have removed our reference to it.

Page 5, lines 20-30: I'm really not a fan of arbitrary/empirical weighting algorithms that are presented as fact without any description of the logic behind the choices that were made and their expected significance.

Although we agree with your assessment on the appearance of arbitrary numbers related to our glint screening, the glint mask used previously in the MISR RA, also the SA, the MODIS and other satellite aerosol-retrieval algorithms, are also arbitrary, are static, and are therefore yet more restrictive. The new weighting is adaptive; it represents a substantial improvement to the original logic and also to the results. We have added the following to the paper: "The minimum and maximum reflectances were taken via forward modeling, and 25° was set as the minimum because, as glitter angle decreases, a small error in wind speed could substantially impact the retrieval. This is a conservative choice; as we improve our ability to determine if a camera is glint-contaminated in the future, we will likely lower this minimum glitter-angle threshold."

Page 8, line 7: Please use a proper citation for that ATBD or relevant paper, not a website.

The citation for the algorithm itself was referred to on line 3, but it may not have been obvious what OBPB refers to; we have clarified this in the references. The website gives a very good description of the algorithm, so we are also leaving the link in the text.

Page 9, line 2: "Spectral coefficients of variation" – this is imprecise wording. IS that the CoV for all of one channel for a patch, added up for all channels?

We explain this on the following line. ‘The spectral coefficients of variation (standard deviation divided by the mean) were calculated for rolling 50 × 50 pixel patches, separately in each spectral band of the nadir camera...’.

Page 9, lines 16-23: Does this mean surface BRDF is assumed to be isotropic? Is that the case?. Also units should be given for the equation on line 17.

This equation is only a scaling of the TOA radiances to produce TOA reflectances, and it retains the angular dependence of the scene. The units of BRDF are sr^{-1} .

Page 10, lines 1-10: Isn't any long term linear trend determined in 3a? Or is this done a year at a time? It is unclear to me from your description.

We subtract out the trend before deseasonalization, which removes the seasonal noise from the signal, and add it back afterward. This allows for a result with much lower uncertainty. We have added this point explicitly to the text.

Page 10, lines 22-24: While I'm sure you're familiar with the Bruegge paper, others may not be. This sentence is quite confusing on its own and needs a more detailed explanation.

This has been clarified with the following:

“The MISR calibration procedure assumes that the panel degrades in a spectrally invariant way. This is likely a poor assumption that produces a spectrally varying TOA reflectance drift with time.”

Page 11, five starting bullets: all of these are arbitrary choices. It would be nice if you had an explanation for your logic in choosing them.

We have added some explanation, but disagree that the choices are arbitrary; they are motivated by the need to use only the highest-quality data for this comparison.

Page 11, five starting bullets: I'm still not following the logic of why MODIS data should be used to screen MISR results, if that is indeed what is happening (its not clear).

MODIS-Terra provides a validated and widely used ocean color product coincident with MISR observations. Here we compare collocated data points for an apples-to-apples comparison. The text now also makes clear that “we mask out any MISR/MODIS data where the MODIS Chl flag data is masked...”.

Page 11, line 10: Here you say you flag out Chl > 1.5, but this is presented in the figures? Do the figures show flagged results removed, or not?

We do present all data with Chl < 10 mg m⁻³, this has been corrected in the text. We tend to focus on the Chl < 1.5 mg m⁻³, as we expect much more sensitivity to retrieved Chl in this regime. This is borne out in the plots.

Page 11, line 16: what is the value of comparing the mean of MISR and MODIS data to SeaBASS?

We have removed the MISR-MODIS mean results from the paper.

Section 4.1: again, I think there are statistical tools you can use that do hypothesis tests that account for sample size. Then you can say in a more quantitative way that the amount of comparison data is “too few” (if it is).

We have commented on this above, and make clear the sample-size limitations.

Section 4.1: You mention in several points that collocated MISR data could improve MODIS retrievals of Chl-a. While I agree that this is probably the case, nothing in the analysis you’ve presented in this paper can demonstrate that.

Providing additional information content to either MISR or MODIS should improve the retrieval. Furthermore, on physical grounds, we expect that the improved “atmospheric correction” would also improve the ocean surface retrieval, particularly near coasts and along aerosol transport pathways over ocean [e.g., Kahn et al., 2016].

Page 12, lines 1-3: Again, comparing MODIS and MISR doesn’t necessarily indicate the correctness of the MISR algorithm. I could envision some situations (probably with low AOT) where MODIS would work better, and others where MISR would. I think if you had parsed Fig 7. to scenes with high and low AOT, or varying Chl-a, you could start to illuminate these issues.

Given a sufficiently large sample size and an uncertainty envelope (obtained from SeaBASS) for MODIS-Terra, one could use MODIS-Terra for a more formal validation. As discussed above, the MISR-MODIS comparison is actually more compelling than the MISR-SeaBASS comparison, because of the very small MISR-SeaBASS sample size, and the validation that has been performed on the MODIS ocean color product. We think stratifying MISR/MODIS Chl results based on AOD and aerosol type is beyond the scope of this paper, but should be considered for future work after validation of the MISR RA AOD and aerosol type is performed.

Page 13, line 11: “substantially better” Is this the case, or is this just a symptom of

correlation coefficients, etc. calculated with far more cases than the SeaBASS comparison.

We have added statistics for the three collocated datasets (MISR, MODIS-Terra, and SeaBASS) to Table 2. We agree it is not possible to definitively say that the statistics are substantially better, and so we have changed the wording accordingly. However, after comparing MODIS-Terra, SeaWIFS, and SeaBASS Chl data from the SeaBASS website, it looks very much like the satellite-remote sensing retrievals are co-varying and that the satellite-remote sensing results agree better with each other than with SeaBASS.

Page 13, line 19: Are coupled retrievals performed for MISR scenes where some cameras observe glint, or are they only computed when all cameras observe a scene? If it's the former, do these retrievals work as well since there are fewer angles? Presumably capability would be degraded – how would this affect the ability to fill in MODIS Terra data in glint?

Yes, coupled retrievals are performed in regions where the nadir (An) camera is in glint. Although we don't have the in-situ comparison to prove this, it is very likely that the uncertainty in the Chl retrieval is tied to the number of cameras used in the retrieval once the glint-contaminated cameras are removed (as well as the viewing geometry of those cameras). The Chl retrieval will probably not be impacted at all by the loss of a "D" camera (70.5° viewing zenith), but the loss of all 3 near-nadir "A" cameras will almost certainly result in higher uncertainty. This is now noted in the text.

Figure 1: I really had a hard time understanding this flowchart. Please try to make it more legible. Minimize text where you can – less is more.

We have learned from reviews of earlier papers that putting the algorithm detail in a flow-chart allows for better understanding of the algorithm with some readers. The structure of the flow chart, and the bolding of some text, is aimed at helping the reader sort out the information. As most readers view our papers digitally these days, an interested reader can zoom in to more easily see the detail, as needed.

Figure 2: It would be nice to remind readers the actual wavelength of the blue and green channels

The numbers are mentioned earlier in the paper, but we have added them here as well.

Figures 4-5: Nobody knows what "Camera Aa", etc. means outside the MISR group. Please just state the viewing angle instead.

We have indicated what the A, B, C, and D camera terminology means in the caption.

Supplementary material

Figure S1: Can you see the colored value of the AERONET sites? I can't.

Yes, we can see it. Because the AERONET values are mapped to the same color scale as MISR, a good match will be difficult to see. Indeed, for the RA, AOD, ANG, Fr. Non-Sph, and SSA all match quite well to AERONET. We have however adjusted the plots so they are easier to interpret.

Only here to you allude to a "part II" of this study. I can only assume that portion will have more details about the coupled RA. Which makes me think that there should really just be two papers, one about calibration, one about coupled retrievals.

We think the calibration is necessary for this work, as discussed above, but we have put it in an appendix.

All supplementary figures: I'm confused why there are consistently fewer MODIS retrievals in some of the scenes, can this be discussed?

MISR runs down the center of the MODIS swath. As the center of the MODIS swath tends to be in sun-glint anywhere near the solar equator, a substantial portion of MISR's swath will have no quality controlled MODIS-Terra Chl retrievals. Because MISR uses up to 9 cameras over ocean, there are always at least a few that will not be contaminated by sun-glint. We have clarified this in the supplemental material.

Updated MISR Dark-Water Research Aerosol Retrieval Algorithm

Part 1: ~~Empirical Calibration Corrections and~~ Coupled 1.1 km Ocean-Surface Chlorophyll-a Retrievals with Empirical Calibration Corrections

James A. Limbacher^{1,2} and Ralph A. Kahn¹

¹Earth Science Division, NASA Goddard Space Flight Center

~~Greenbelt MD, 20771, USA~~

²Science Systems and Applications Inc., Lanham ~~MD, 20706, USA~~

~~For: Atmospheric Measurement Technologies~~

~~Submitted: October 2016~~

Style Definition: Normal: Font: 10 pt, Justified, Line spacing: 1.5 lines

Style Definition: Header: Font: 10 pt, Justified, Line spacing: 1.5 lines, Tab stops: 8 cm, Centered + 16 cm, Right + Not at 7.62 cm + 15.24 cm

Style Definition: Hyperlink: Font color: Blue

Style Definition: List Paragraph: Font: 10 pt, Justified, Line spacing: 1.5 lines

Style Definition: Balloon Text: Font: (Default) Tahoma, 8 pt, Justified

Style Definition: Footer: Font: 10 pt, Justified, Tab stops: 7.96 cm, Centered + 15.92 cm, Right + Not at 7.62 cm + 15.24 cm

Formatted: Font: 10 pt

Formatted: Font: 17 pt

Formatted: MS title, Left, Right: 0

Formatted: Font: 17 pt

Formatted: Font: 17 pt, Not Bold, Font color: Auto

Formatted: Authors, Left, Right: 0

Formatted: Affiliation, Left, Right: 0 cm

Formatted: Affiliation, Left, Right: 0 cm

Formatted: Font: Times New Roman, Font color: Auto

Formatted: Font: Times New Roman, Font color: Auto

Formatted: Font: Times New Roman, Font color: Auto

Correspondence to: Ralph A. Kahn (ralph.a.kahn@nasa.gov)

Abstract

As aerosol amount and type are key factors in the “atmospheric correction” required for remote-sensing chlorophyll-a concentration (*Chl*) retrievals, the Multi-Angle Imaging Spectroradiometer (MISR) can contribute to ocean color analysis despite a lack of spectral channels optimized for this application. Conversely, an improved ocean-surface constraint should also improve MISR aerosol-type products, especially spectral single-scattering albedo retrievals. ~~We~~ We introduce a coupled, self-consistent retrieval of *Chl* together with aerosol over dark water. There are time-varying MISR radiometric calibration errors that significantly affect key spectral reflectance ratios used in the retrievals. Therefore, we also develop and apply new calibration corrections to the MISR top-of-atmosphere (TOA) reflectance data, ~~and introduce a self-consistent retrieval of *Chl* together with aerosol over dark water. The calibration corrections include: a modified stray-light model based on comparison~~ comparisons with coincident MODerate resolution Imaging Spectroradiometer (MODIS) Terra data, observations and trend analysis ~~using of the~~ MISR TOA bidirectional reflectance factors (BRFs) over three pseudo-invariant desert sites. ~~The trend analysis shows that MISR radiometric sensitivity decreased by up to 2 percent for MISR spectral bands between January 2002 and December 2014.~~

~~After applying calibration corrections, we~~ We run the MISR Research Retrieval Algorithm (RA) ~~to validate with the corrected MISR RA reflectances to generate MISR-retrieved *Chl*, and analyze both~~ compare the MISR ~~and corresponding MODIS Terra *Chl* values compared to a set of 49 collocated coincident SeaBASS *in-situ* observations, constrained to~~ Where $Chl_{in-situ} < 1.5 \text{ mg m}^{-3}$. Statistically, compared to the validation data, MODIS demonstrates a higher ~~results from our *Chl* model are expected to be of highest quality, due to algorithmic assumption validity. Comparing MISR RA *Chl* to the 49 coincident SeaBASS observations, we report a correlation coefficient (r) of 0.91 vs. 0.86 for MISR, a lower root-mean-squared-error (RMSE) of 0.25 vs. 0.22, but a higher, and a median absolute error (MAE) of 0.14 vs. 0.10. Because 49 data points are insufficient to draw strong conclusions, we~~ Statistically, a two-sample Kolmogorov-Smirnov test indicates that it is not possible to distinguish between MISR *Chl*, and available SeaBASS *in situ Chl* values ($p > 0.1$). We also compare MODIS Terra and MISR RA *Chl* statistically, over much broader regions. With about 1.5 million MISR-MODIS collocations having MODIS $Chl < 1.5 \text{ mg m}^{-3}$, MISR and MODIS show very good agreement: $r=0.96$, MAE=0.09, and RMSE=0.15. MISR-MODIS agreement is substantially better than the 49 data point MODIS-SeaBASS comparison, indicating that MISR *Chl* retrievals might complement MODIS, especially after further upgrades are made to the MISR RA ocean color model.

~~The new dark water aerosol/*Chl* RA can retrieve *Chl* in low-*Chl* (<1.5), case I waters, independent of other imagers such as MODIS, via a largely physical algorithm, compared to the commonly applied statistical ones. At a minimum, MISR’s unique multi-angular angle data can better constrain aerosol type, helping should help reduce uncertainties in the MODIS Terra Ocean color retrieval, and suggesting how where coincident measurements are made, while also allowing for a joint MISR-MODIS over-ocean algorithm might exceed the capabilities more robust retrieval of either instrument alone. particle properties such as spectral single-scattering albedo.~~

Formatted: Font: Times New Roman, 10 pt, Font color: Auto

Formatted: Default Paragraph Font

Formatted: Right: 0 cm

Formatted: pb_abstract

Formatted: pb_abstract

Formatted: Font: Italic

Formatted: Font: Italic

Formatted: Default Paragraph Font

1. Introduction

Among the geophysical quantities routinely produced from the NASA Earth Observing System's Multi-angle Imaging SpectroRadiometer (MISR) instrument are aerosol optical depth (AOD) and aerosol type. ~~MISR's unique~~ MISR measures upwelling short-wave radiance from Earth in four spectral bands centered at 446 (blue), 558 (green), 672 (red), and 866 nm (near-infrared, or NIR), at each of nine view angles spread out in the forward (f) and aft (a) directions along the flight path, at 70.5°, 60.0°, 45.6°, 26.1°, and nadir [Diner et al., 1998]. The three near-nadir cameras are designated "Af," "Aa," and "An," and successively steeper-viewing pairs are "B," "C," and "D" cameras. MISR's multi-angle, multi-spectral radiance data sample air-mass-factors ranging systematically from one to three, making AOD retrieval possible even over bright desert surfaces, and improving retrieval sensitivity at low AOD compared to single-view instruments. In low-AOD situations, which are common over ocean, poor representation of the surface reflectance can limit aerosol retrieval accuracy, as the relative contribution of ocean under-light can be large, especially at shorter wavelengths. Therefore, applying a physical retrieval to constrain the ocean surface reflectance, of interest in itself as an indicator of ocean biological activity and its impact on the global carbon cycle (e.g., Behrenfeld et al., 2006), should also reduce the uncertainties in the concomitant aerosol retrievals, assuming that the aerosol and ocean signals do not co-vary substantially over MISR's 36 channels.

A second factor directly affecting the quality of almost every MISR geophysical data product is the accuracy of the instrument's radiometric calibration. ~~Calibration includes determination of (1) the absolute radiometric scale, as well as (2) the relative band to band response among the four MISR spectral bands, (3) camera to camera response among the nine MISR cameras, (4) flat fielding across the MISR imagery, and (5) temporal trends in these quantities. Considerable effort has been expended to assess MISR radiometric calibration and to meet the standards of approximately 3% absolute and 1% channel to channel, established pre-launch. This work involved pre-launch laboratory studies [Bruegge et al., 1999], on board calibrator analysis and lunar calibration, along with vicarious calibration over bright land targets [Bruegge et al. 2004; 2007; 2014], symmetry tests comparing the forward and aft viewing cameras across the solar equator [Diner et al., 2004], and over ocean dark target vicarious calibration [Kahn et al., 2005]. Cross-calibration analysis has been performed over bright and dark land and ocean surfaces with the MODerate-resolution Imaging Spectroradiometer (MODIS), that flies aboard the Terra satellite with MISR [Lyapustin et al., 2007], and MODIS combined with the MEdium Resolution Imaging Spectrometer (MERIS), the airborne AirMISR instrument, and the Landsat 7 ETM+ [Bruegge et al., 2007], and the Polarization and Directionality of the Earth's Reflectances 2 (POLDER 2) [Lallart et al., 2008]. A synthesis of much of this work is given in Bruegge et al. [2014].~~

As the MISR data record now exceeds 1617 years of near-global coverage about once per week, the advantages of further refining the MISR calibration have increased multifold. This applies to determining AOD trends, and is especially true in the context of MISR's unique ability to retrieve aerosol type (Kahn and Gaitley, 2015). In addition to AOD and aerosol type, retrievals of ocean bio-optical properties from space are extremely sensitive to the calibration of the instrument, because only 5 to 20% of the top-of-atmosphere (TOA) reflected signal in the blue and green spectral bands, where ocean color is retrieved, arises from scattering related to ocean under-light (e.g., Gordon and Wang, 1994). To retrieve this signal, the following must be properly accounted for: (1) molecular (Rayleigh) scattering, (2) molecular absorption, (3) scattering from

Formatted: Font: 12 pt

Formatted: Font: 12 pt

Formatted: Font: 12 pt, Not Bold

Formatted: Heading 1, Right: 0 cm

Formatted: Right: 0 cm

Formatted: Font: Not Italic

Formatted: Font: Not Italic

Formatted: Right: 0 cm

Formatted: Font: Not Italic

atmospheric aerosols, (4) absorption from atmospheric aerosols, (5) reflection from foam and whitecaps, and (6) Fresnel reflection (glint) from the ocean surface. Of course, the aerosol and molecular signals include both an atmospheric path radiance term and a term with at least 1 surface reflection. In earlier work, we used image analysis, including comparisons with coincident MODIS observations, to identify empirical relationships that correct anomalies exhibiting spatial structure in high-contrast scenes, an aggregate of “ghosting” light reflections (or stray light) within the cameras. We make minor adjustments to our earlier ghosting and flat fielding (CCD detector based gain errors, which will show up as across track biases in reflectance) corrections for the results presented in this paper, but the underlying work for these corrections is found in *Limbacher and Kahn [2015]*. In the course of this analysis, we also observed some systematic, temporal drift in the measured reflectances. Addressing this calibration trend is a major focus of the current paper, as along with highlighting our ability to retrieve chlorophyll a (*Chl*) and aerosol amount/type self-consistently with the corrected MISR reflectances, using an improved version of the MISR dark water MISR research algorithm (RA). The paper is organized as follows: section 2 reviews the datasets used in our analysis and the methodology adopted, section 3 addresses the observed temporal trends in MISR radiometric calibration from 2002 to 2015, section 4 presents the *Chl* retrievals and initial validation of the results, and conclusions are given in section 5 (e.g., Figure 2; more generally, Gordon and Wang, 1994). We find that not only the absolute radiometric calibration, but also the MISR blue/green ratio, critical for ocean color applications, has changed over time.

2. Comparison datasets and methodology

This paper is organized as follows: section 2 reviews the datasets used in our analysis and the methodology adopted, section 3 presents the *Chl* retrievals and initial validation of the results, example retrievals are shown in section 4, and conclusions are given in section 5. MISR radiometric calibration corrections, including details of the observed temporal trends, are described in Appendix A.

2 Comparison datasets and methodology

2.1 The MISR Research Algorithm, with Enhanced Ocean Reflectance Model (RA)

The aerosol/*Chl* retrieval algorithm is summarized as a flow chart in Figure 1. An in-depth description of the current main RA components can be found in *Limbacher and Kahn [2014; 2015]*. Briefly, the algorithm finds the set of aerosol optical models, and associated aerosol amounts, and *Chl* values, that minimize the difference between the observed TOA reflectances (identical to BRFs described in section 3 Appendix A, but without the solar-zenith-angle normalization) and simulated values that are stored in a look-up table (LUT). The overall aim is to derive AOD and *Chl* over 1.1 km retrieval regions, conditioned on aerosol-type mixtures that produce TOA reflectances that meet certain χ^2 criteria. In the current study, we compare the MISR RA *Chl* retrievals to coincident validation data taken at the surface, after all MISR

Formatted: Heading 2, Right: 0 cm

Formatted: Font: Not Bold

Formatted: Font: Not Italic

calibration corrections are applied (Appendix A), and also identify the impact the refined ocean surface model has on the retrieved aerosol results for a few scenes, in Section 4 below.

2.2 MISR RA Enhanced Ocean Reflectance Model

Prior to Limbacher and Kahn (2014), the MISR RA simulated ocean surface ~~is~~ modeled as ~~a black, an~~ isotropic (wind-speed-dependent only) Fresnel-reflector, (Cox-Munk), with whitecap reflectance included. ~~Additionally, In Limbacher and Kahn (2014), we made~~ adjustments to the whitecap reflectance, and ~~added an ocean~~ under-light ~~due to term that includes~~ molecular scattering, ~~colored dissolved organic matter (CDOM) and Chl were previously modeled using and particulate attenuation. In Limbacher and Kahn (2014, 2015), we used~~ wind and ocean-color constraints from the Cross-Calibrated Multi-Platform (CCMP; Atlas et al., 2011) and GlobColour ~~{(Barrot et al., 2010)2014}~~ products, ~~respectively, (and from~~ climatology where these products were unavailable), ~~respectively, to prescribe the ocean's color.~~

For the current analysis, we continue using CCMP data for 10-meter wind speed (where available, otherwise we use the MISR Standard Algorithm (SA) wind data), ~~and we, which comes from monthly averaged values of QuikSCAT and SSM/I (Michael Garay, personal communication).~~ We set the surface pressure to 1013.25 mb, as we find a number of cases where the MISR Standard Product surface pressure over ocean is aliased from nearby mountains. ~~This results from the different footprint sizes of the SA vs. the RA; the SA has a 17.6 km footprint, whereas the RA has a 1.1 km footprint.~~ Additionally, ~~instead of prescribing Chl,~~ we now ~~retrieve it directly in the algorithm by inverting our ocean color model. To do this, we~~ use all four MISR spectral bands to simultaneously retrieve aerosol and Chl, with equal weighting, whereas the SA ~~{(Martonchik et al., 2009)}~~ and past versions of the RA ~~retrieved only aerosol amount and type, and~~ used only the red and NIR bands ~~(except at high AOD),~~ where the ocean surface is darkest, ~~except at high AOD.~~ However, ~~empirical camera~~ weighting is applied to mitigate the effects of sun glint, and different uncertainties are assigned to the 36 MISR channels when evaluating the χ^2 acceptance criteria, as discussed below. ~~Generally, the near-nadir views and shorter wavelength bands contain more information about the surface, whereas the steeper views tend to provide greater constraint on the atmospheric aerosols. A refinement to the algorithm, not implemented here, would be to separate the Chl and aerosol retrievals, so we can weight contributions from each channel in a manner that reflects the differences in information content. CDOM absorption is assumed to co-vary with Chl (Morel and Gentili, 2009).~~

~~Colored dissolved organic matter (CDOM) absorption is assumed to co-vary with Chl (Morel and Gentili, 2009).~~ Relationships connecting Chl to absorption and back-scattering coefficients can be found in many places; the ones we used (Chen et al., ~~{2010}; 2003;~~ Devred et al., ~~{2006};~~ Morel and Prieur, ~~{1977};~~ Morel ~~{1988}~~) are summarized in Sayer et al., ~~{2010}~~. For our ocean under-light model, we modify the absorption of light by seawater for the blue spectral band from the Morel and Prieur ~~{1977}~~, which was used previously in the RA, to more recent results from Lee et al., ~~{2015}~~.

The following equation gives a bidirectional water-leaving radiance:

$$L_w^+(m_0, m, Df, l, WS, t, mix, Chl) = E_d(m_0, l, t, mix) * \mathfrak{R}(m, WS) * \left(\frac{b_b(l, Chl)}{a(l, Chl)} \right) * \frac{f}{Q}(m_0, m, Df, l, Chl)$$
$$L_w^+(m_0, m, Df, l, WS, t, mix, Chl) = E_d(m_0, l, t, mix) * \mathfrak{R}(m, WS) * \left(\frac{b_b(l, Chl)}{a(l, Chl)} \right) * \frac{f}{Q}(m_0, m, Df, l, Chl) \quad (1)$$

Formatted: Right: 0 cm

Formatted: Font: Not Italic

Formatted: Font: Not Italic

Formatted: Font: Not Italic

Formatted: Right: 0 cm, Tab stops: Not at 15.08 cm

Formatted: Font: Not Italic

Formatted: Right: 0 cm

Formatted: Right: 0 cm

The following explanation of the terms in equation (1) is basically a summary of Morel et al. (2002), which is also where the LUT for f/Q and \mathcal{R} was obtained. Variable dependences are included here only if they are given in the Morel et al. (2002) LUT.

Formatted: Font: Not Italic

Formatted: Font: Not Italic

- L_w^+ represents the water-leaving radiance, which is the upward-directed radiance just above the water surface (excluding sun-glint). It is a function of the cosine of the solar zenith angle (μ_0), the cosine of the view (camera) zenith angle (μ), the relative azimuth between the sun and the sensor ($\Delta\phi$), the wavelength (λ), the wind speed (WS), the total column optical depth (τ), aerosol optical model (mix), and Chlorophyll-a concentration (Chl).
- E_d represents the downward directed solar irradiance at the bottom of the atmosphere.
- \mathcal{R} is a reflectance factor, the product of two effects: the fraction of the downward directed bottom-of-atmosphere irradiance (E_d) transmitted through the air-sea interface, and the fraction of the upward directed radiance from just beneath the air-sea interface transmitted through the interface.
- b_b represents the total backscattering coefficient of the water plus other material within the water.
- a represents the total absorption coefficient of the water plus the other material within the water.
- f represents an empirical correction to the ratio of the backscattering to absorption (essentially a modification to the upward directed under-light irradiance).
- Q represents the ratio of the upward-directed irradiance to radiance just below the air-sea interface. This term (along with f) is responsible for creating the directional dependence of the under-light on solar and viewing geometry.

Formatted: Indent: Left: 0.63 cm, Hanging: 0.63 cm, Right: 0 cm

L_w^+ is multiplied by the transmittance from the bottom of atmosphere to the camera ($T_{a,up}$) to get the surface contribution to the TOA reflectances. Because the integrated water-leaving radiance, $L_w^+ \ll E_d$ (i.e., the under-light albedo is small), the probability that a photon will be multiply reflected due to under-light is very small, regardless of atmospheric loading, and is ignored, given other, larger uncertainties in the algorithm. However, multiple surface reflections due to sun-glint and whitecaps are directly accounted for in the radiative transfer code.

Formatted: Right: 0 cm

~~Initial processing of the MISR radiances includes adjusting and applying our ghosting parameterization, and correcting for flat fielding and for temporal degradation in the calibration (see Section 3 below). We then revise the band-to-band calibration by increasing the red reflectance 0.75% and decreasing the near-infrared (NIR) reflectance 0.75%, adjustments that are within the calibration uncertainty and are required to match a global set of coincident, spectral aerosol optical depth validation data [Limbacher and Kahn 2014; 2015]. We also apply corrections to the radiance data to smooth out apparent anomalies in the instrument gain, based on Bruegge et al. [in preparation].~~

Formatted: Font: Not Italic

As we aim to extract both surface and aerosol information from the MISR data, we apply new camera weights when calculating the χ^2 test variables used to assess the agreement between the observed reflectances and those derived for various aerosol component and mixture options. In the SA and previous versions of the RA, a glitter mask was applied arbitrarily to all cameras viewing within 40° of the specular direction. Instead, we now use a combination of glitter-angle and Rayleigh NIR reflectance, calculated assuming $Chl = 0.1 \text{ mg/m}^3$ to assess glint-contamination in each camera. The new camera weights are the product of the following two empirically derived equations:

Formatted: Right: 0 cm

$$\rho_{weight,i} = 1.0 - \min \left\{ \max \left[\frac{(\mu_i \rho_{model,i}^{NIR} - 0.0075)}{0.0125 - 0.0075}, 0.0 \right], 1.0 \right\}, \quad (2)$$

$$glitter_{weight,i} = \min \left\{ \max \left[\frac{(G_i - 25.0)}{40.0 - 25.0}, 0.0 \right], 1.0 \right\} \quad (3)$$

Here ρ_{model}^{NIR} represents the modeled NIR Rayleigh reflectance over an ocean surface for a particular MISR camera (i), and G is the glitter angle relative to the same MISR camera. The minimum and maximum reflectances were taken via forward modeling, and 25° was set as the minimum because as glitter angle decreases, a small error in wind speed could substantially impact the retrieval. Equation 2 returns a value of unity if the modeled NIR reflectance is ≤ 0.0075 , ~~decreasing; this weight decreases~~ linearly to zero if the modeled reflectance is ≥ 0.0125 . Essentially, as the modeled glint strength increases, camera weighting decreases. Similarly, Equation 3 produces a value of unity if the glitter angle $\geq 40^\circ$, decreasing linearly to zero for $G \leq 25^\circ$. The product of these weights provides better glint masking than using an arbitrary cutoff, and the quality of these new weights should improve with the quality of the input wind speed data. Further, as we improve our ability to determine if a camera is glint-contaminated in the future, we will likely lower this minimum glitter-angle threshold.

~~The aerosol/Chl retrieval process is summarized as a flow chart in Figure 1. Essentially, the Chl retrieval can be thought of as an inversion of our ocean under light model (i.e., instead of prescribing Chl, we retrieve it). The overall aim is to derive AOD and Chl over 1.1 km retrieval regions, conditioned on aerosol type mixtures that produce TOA radiances that meet certain χ^2 criteria. In the current study, we compare the MISR RA Chl retrievals, after all MISR calibration corrections are applied, to coincident validation data taken at the surface, and also identify the impact the refined ocean surface model has on the retrieved aerosol results. In the RA pre-processing, all MISR L1B2 reflectance data are first averaged to 1.1 km. The reflectances are then rotated to the L1B1 format as described in Limbacher and Kahn [2015] and updated stray light and flat-fielding corrections are applied before being rotated back to L1B2 format. Compared to Limbacher and Kahn [2015], we modify the stray light corrections in the following way:~~

- ~~• The primary ghost term has been divided into a discrete ghosting component (reflected images of features in the scene) and an unstructured veiling light component.~~
 - ~~○ This revised primary ghost has a band and camera dependent along track offset applied, as indicated by MISR lunar observations acquired on 14 April 2003 [e.g., Bruegge et al., 2004].~~
 - ~~○ The primary ghost image is also stretched/squeezed across track (for the near nadir “A” cameras only), based on further comparisons with MODIS Terra, following the same approach as our earlier work.~~
- ~~• Via ray tracing, it was found that the “secondary ghosting” term in Limbacher and Kahn [2015] distributes light uniformly from the left or right most 1/3 of the scene to the remainder of that half of the scene [Ab Davis, personal communication, 2016], and the correction has been modified accordingly.~~
- ~~• All stray light terms are now represented as convolutions, which are much quicker to compute than applying the functions pixel by pixel as was done in our earlier work.~~
- ~~• The magnitudes of all stray light terms have been adjusted as a result of adding the unstructured veiling light component.~~
- ~~• The stray light model for the AN camera (all four bands) is used for all off nadir cameras. Only the along track offset and primary ghost stretching are varied by camera.~~

Figure 2 illustrates the impact of including under-light in the MISR RA, for the blue and green-band retrieval TOA reflectance results. For this figure, MISR aerosol retrievals over dark water were performed using the multi-angular data

Formatted: Right: 0 cm

Formatted: Indent: Hanging: 0.63 cm, Right: 0 cm

Formatted: Font: Not Italic

Formatted: Indent: Hanging: 0.63 cm, Right: 0 cm

Formatted: Right: 0 cm

~~only~~ for the NIR band only, because the ocean surface tends to be darkest at this wavelength, ~~as (i.e., where~~ under-light makes its smallest spectral contribution~~).~~ When the retrieved aerosol properties are used in the forward radiative transfer model to simulate the MISR top-of-atmosphere (TOA) reflectances in the blue and green bands, but under-light is not included, there are large discrepancies in the modeled TOA reflectances compared to the original MISR observations (Figure 2, top two panels). However, when under-light is accounted for in the simulations (in this illustration using coincident MODIS Terra *Chl* as input), the biases are substantially reduced, as shown in the lower two panels of Figure 2. As the MODIS-constrained *Chl* was included when the aerosol retrieval was performed (~~with~~using only the multi-angle NIR data ~~only~~), this example demonstrates the magnitude of the surface contribution to the TOA reflectances in the blue and green spectral bands. If surface contributions are not explicitly included, the aerosol retrievals would be skewed, and the spectral dependence of the anomaly ~~would have a large effect on~~could impact the derived aerosol type (e.g., Kahn and Gaitley, 2015~~),~~ especially when the blue or green bands are included in the aerosol retrieval. In Section 4 ~~and supplemental material~~ we demonstrate the use of MISR to constrain *Chl* self-consistently with the retrieval of aerosol over ocean. ~~However, we first refine the calibration of MISR, as described in section 3.~~

Formatted: Font: Not Italic

2.2 MODIS Terra top-of-atmosphere reflectances

Formatted: Font: Not Bold

Formatted: Heading 2, Right: 0 cm

The MODIS TOA reflectances are key to several radiometric calibration adjustments detailed in Appendix A. As in Limbacher and Kahn (2014), MODIS-Terra equivalent reflectance data are used as a baseline to compare against MISR, especially for the near-nadir ~~cameras~~camera. We use the latest MODIS collection 6 TOA reflectances (Sun et al., 2012) with additional corrections implemented via an algorithm provided by Alexi Lyapustin (Lyapustin et al., 2014; elaborated in Limbacher and Kahn, 2015). Primarily, we are interested in the following MODIS bands: 9 (443 nm, as compared to MISR's 446 nm blue), 4 (555 nm, as compared to MISR's 558 nm green), an average of bands 13 and 14 (effectively 672 nm, as compared to MISR's 672 nm red), and 2 (856 nm, as compared to MISR's 866 nm NIR). In the current study, MODIS reflectances are used only to remove flat-fielding artifacts in the MISR imagery and to make modifications to the ghosting parameterization described in Limbacher and Kahn (2015), so the absolute calibration accuracy of MODIS is not critical here. ~~For the flat fielding characterization, we select only low contrast scenes, where ghosting artifacts are minimal, and we then normalize the mean MISR-MODIS ratios for the entire scene to unity. For the ghosting modifications, we normalize the MISR-MODIS ratios to an area of little contrast, where stray light is unlikely to be a problem.~~ The most critical assumptions are that MODIS swath-edge and scan-angle issues are minimal for the scenes of interest, and that pixel-to-pixel relative precision is high. Fortunately, because the MISR swath samples about 380 km around the center of the 2,300 km MODIS swath, the effects of MODIS swath-edge and scan-angle artifacts on the coincident data are minimal.

Formatted: Right: 0 cm

Formatted: Font: Not Italic

2.3 The SeaWiFS Bio-optical Archive and Storage System (SeaBASS) data set

Formatted: Heading 2, Right: 0 cm

Formatted: Font: Not Bold

The SeaBASS dataset (Werdell et al., 2002; <https://seabass.gsfc.nasa.gov>) was originally developed to compare products retrieved from sensors such as the Sea-viewing Wide Field-of-view Sensor (SeaWiFS) and MODIS with in-situ bio-optical observations. We use SeaBASS chlorophyll validation data generated either by fluorometry or by high-performance liquid chromatography (HPLC). Uncertainties for HPLC and fluorometry *Chl* measurements are 5% and 8%, respectively

Formatted: Right: 0 cm

Formatted: Font: Not Italic

Formatted: Font: Not Italic

Formatted: Font: Not Italic

Formatted: Font: Italic

(Heukelem et al., 2002). If HPLC (*Chl*) and fluorometry (*Chl*) data were acquired at the same location and time, we use the HPLC (*Chl*) data; otherwise we use ~~whichever the fluorometry data are available~~. Because the MISR Standard Algorithm does not retrieve *Chl*, the MISR-SeaBASS coincidences were found by locating MODIS-Terra validation matchups (Bailey and Werdell, 2006) and setting the viewing-zenith angle maximum to 16°, which corresponds to the edge of the MISR nadir (AN) camera field-of-view. ~~In addition, To assure meaningful SeaBASS observations for MISR *Chl* validation purposes, we also applied the following criteria:~~ (1) minimum sea floor depth was set to 30 meters to mitigate errors due to sea floor reflections, especially in the blue band, (2) maximum wind speed was set to 7 m/s to avoid whitecaps (eliminating ~25% of data), (3) maximum solar zenith angle was set to 70° ~~to eliminate steep-incidence-angle effects~~, (4) maximum coefficient of variation for MODIS *Chl* was set to 0.15 ~~to avoid aliasing due to spatial variability of the scene~~, (5) maximum SeaBASS-MISR time difference was set to 3 hours, and (6) minimum number of valid MODIS pixels was set to 25% ~~resulting in%~~. ~~This produced~~ 75 coincidences that have valid MISR aerosol/*Chl* retrievals. Of these 75 coincidences, ~~only about 5049~~ correspond to *Chl* < 1.5 ~~(the *Chl* regime where the MISR retrievals are expected to show good performance)~~, and also have at least one valid MISR RA retrieval in a 5.5 x 5.5 km area surrounding the SeaBASS station passing our quality tests.

Formatted: Font: Not Italic

Formatted: Font: Not Italic

2.4 MODIS Terra Chlorophyll-a

Formatted: Font: Not Bold

Formatted: Heading 2, Right: 0 cm

Although we validate our *Chl* retrieval against the SeaBASS dataset for *Chl* < 1.5, we also cross-compare our *Chl* results with ~~those from~~ MODIS-Terra (OBPG, OB.DAAC; 2014) to increase the number of coincidences (especially needed for *Chl* < 1.5), and because MISR and MODIS share a common platform. This ensures that the solar geometry is the same for MODIS and MISR, and minimizes potential collocation errors. To do this, we compare MISR RA-retrieved *Chl* with the corresponding MODIS Terra retrieved values ~~(Hu et al., 2012)~~. Details of the algorithm used to generate the MODIS data can be found at http://oceancolor.gsfc.nasa.gov/cms/atbd/chlor_a. Briefly, a training dataset containing collocated *in situ* *Chl* and spectral water leaving radiance (L_w^+) is used to empirically relate the ratio of blue-to-green MODIS L_w^+ to near-surface *Chl* ~~(Werdell and Bailey, 2005)~~. This same relationship is then used to retrieve MODIS *Chl* elsewhere, although the quality of the result also depends in part on the quality of the associated atmospheric correction ~~(e.g., Kahn et al., 2016)~~.

Formatted: Right: 0 cm

Formatted: Font: Not Italic

Formatted: Font: Not Italic

Formatted: Font: Not Italic

2.5 The Aerosol Robotic Network (AERONET)

Formatted: Heading 2, Right: 0 cm

Formatted: Font: Not Bold

Although the main purpose of this paper is to demonstrate and validate our *Chl* retrieval, we also compare the new algorithm against Aerosol Robotic Network (AERONET) observations ~~(in the supplemental material)~~ for a few selected scenes. AERONET sun photometers ~~(Holben et al., 1998)~~ provide very accurate measurements of AOD ~~(Eck et al., 1999)~~ and Ångström exponent (ANG). The almucantar inversions ~~(Dubovik and King, 2000)~~ can provide constraints on particle sphericity (Dubovik et al., 2006; which we convert to fraction mid-visible AOD assigned to non-spherical particles, or Fr. Non-sph), and aerosol single scattering ~~albedos (SSA)~~ albedo (SSA), provided the aerosol loading is high: (AOD at 440 nm > 0.4), the scattering angle range for the inversions is large, and the aerosol is relatively uniform over the range of view angles used for the inversion ~~(Holben et al., AERONET's Version 2.0 quality assurance criteria)~~.

Formatted: Right: 0 cm

Formatted: Font: Not Italic

Formatted: Font: Not Bold

Formatted: Font: 14 pt, Bold

3. Temporal Trends in the MISR Calibration

Formatted: Font: 12 pt, Not Bold

As all aspects of the MISR calibration, in addition to correction for high-contrast scene artifacts, can affect retrieval products such as aerosol type and ocean surface properties [Limbacher and Kahn, 2015], we identify here temporal trends in the instrument calibration, again using an empirical image analysis approach. Bruegge et al. [2014] identified temporal trends in the MISR bidirectional reflectance factor (BRF, computed as described in Step 1a. below) data, based on a time series of mean BRFs for a region approximately 10×20 high resolution (275-m) MISR pixels (roughly 2.5×6 km) in size, centered at (27.21° N; 26.10° E) within the Egypt 1 stable desert site. Although this site is stable over time, we adopt a different methodology, similar to Lyapustin et al. [2014], using average BRFs over larger areas at three stable desert sites (Egypt 1, Libya 1, and Libya 4). Both techniques are valid, but given the homogeneity of the selected sites, we limit geo-location error by averaging, and we reduce the influence of clouds by selecting the median BRF pixel from each case.

Formatted: Font: Not Italic

Formatted: Font: Not Italic

The first challenge to performing the temporal trend analysis is finding suitable homogeneous regions. The following was done to select study regions within each of the three sites: (a) The spectral coefficients of variation (standard deviation divided by the mean) were calculated for rolling 50×50 pixel patches, in each spectral band of the nadir camera, for three or more orbits. (b) The 50×50 pixel patch having the smallest maximum coefficient of variation among the selected orbits and the four spectral band values was chosen for subsequent time-series analysis. The central coordinates for the sites selected are: Egypt 1 (26.62° N, 26.18° E), Libya 1 (24.73° N, 13.52° E), and Libya 4 (28.77° N, 23.50° E). Information about these calibration sites can be found at http://calval.cr.usgs.gov/rst-resources/sites_catalog/radiometric_sites/test_site_gallery/.

Formatted: Right: 0 cm

The central coordinate of each study site is imaged repeatedly by MISR along at least two distinct paths having different sub-spacecraft ground tracks, and therefore different viewing geometries at the site. (A "path" is one of 233 ground tracks that the Terra satellite covers, repeatedly, every 16 days.) So the following procedure was applied separately to each path and camera (6 paths \times 9 cameras), for data acquired between January 1, 2002, and December 31, 2014, giving 13 full years of MISR data. (Prior to January 1 2002, the spacecraft equator crossing time was not yet stable, so viewing geometry varied too much for this time-series analysis.) All observations of each site, about four per month, were initially included. Note that we also apply flat-fielding corrections [Limbacher and Kahn, 2015], and additional corrections to the radiance data to smooth the instrument gain temporal samples (Carol Bruegge, personal communication, 2016).

Formatted: Right: 0 cm

1) Calculate median patch reflectance for each orbit

- a. Perform Earth-Sun and solar zenith normalization according to: $BRF = L * (\pi * D^2) / [E(i) * \cos(SZA)]$, where L is the top of atmosphere radiance, D is the sun-Earth distance in AU, E(i) is the band-weighted exo-atmospheric solar irradiance for band (i), and SZA is the solar zenith angle.
- b. Calculate the median (and mean) BRF and standard deviation over a region 25 km in radius surrounding the central latitude/longitude coordinate.

- c. ~~If the wavelength maximized coefficient of variation is less than 0.02, save the median BRF for use in the time series, otherwise discard the data.~~

~~Median BRF values for at least 193 orbits, and up to 229 orbits, were retained for all 6 paths, 4 spectral bands, and 9 cameras at this step.~~

2) ~~Remove outliers for each path/site and spectral band~~

- a. ~~Arrange the saved median BRFs by acquisition date, fit a line to the values, and subtract the linear trend from the data.~~
- b. ~~Aggregate the data by day of year (DOY) and smooth the sorted, de-trended BRFs using a 21-point (i.e., ± 10 data point) rolling average. (The data are sufficiently dense that replacing each data point with the mean of 21 points does not create significant artifacts in the time series.)~~
- c. ~~a. Identify BRFs that fall outside 2σ from time series.~~
- d. ~~b. Remove the identified outliers from the original data.~~

~~This step removed 3–14% of data outliers from each time series.~~

3) ~~De-seasonalize the data for each site and spectral band~~

- a. ~~Fit a line to the original, time-ordered BRFs, with outliers removed, and linearly de-trend the data.~~
- b. ~~Re-aggregate the data by DOY and smooth the BRFs again using a 21-point (± 10 data point) rolling average.~~
- c. ~~a. Rearrange the data by time and add back the linear trend from Step 2a.~~

~~Step 3 is illustrated in Figure 3 for the Libya 4 site.~~

4) ~~Normalize the data~~

- a. ~~Normalize the data so the time series mean for each spectral band at each site is 1.0, allowing data from multiple sites and paths to be compared. The result is 216 normalized time series, one for each MISR camera and band, for each of two paths at three sites.~~
- b. ~~These time series are then aggregated across all paths to produce 26 time series, one for each MISR channel (Figure 4).~~

~~The linear percent change per decade and its 95th percent confidence interval are then calculated for each channel, and the results are presented in Table 1 and Figure 5. The trends are all negative, as might be expected due to sensor degradation over time. They are smallest in the blue band for all but the forward-viewing 70.5° (Df) and 60.0° (Cf) cameras, smallest for the aft-viewing 70.5° (Da) and 60.0° (Ca) cameras for all bands except the NIR, and largest for the An, and 26.1° forward (Af) and aft-viewing (Aa) cameras. The largest drift overall is about 1.5% per decade for the AN camera red and NIR bands, and the uncertainty in these results ranges from 0.1% per decade to 0.4% per decade, depending on wavelength and camera. The apparent stability of the MISR blue band is probably due to the use of the blue diode to assess degradation of the MISR on-board calibration panels, that is subsequently applied to panel degradation in the other spectral bands for all cameras [Bruegge et al., 2007].~~

4. Validation of MISR RA *Chl* retrievals against SeaBASS, and comparisons with MODIS

Formatted: Right: 0 cm

Formatted: Right: 0 cm

Formatted: Right: 0 cm

Formatted: Right: 0 cm

Formatted: Heading 1, Right: 0 cm

Formatted: Font: 12 pt

Formatted: Font: 12 pt, Not Bold

Collocation of the MISR and SeaBASS observations is of course critical to achieving meaningful comparisons. So for each SeaBASS-MISR coincidence, the corresponding location within a MISR orbit is identified as a block (180 blocks per orbit), line (128 along-track lines per block), and sample (512 across-track samples per block) at 1.1×1.1 km. We run the RA, as described in section 2.2, over three blocks of data per coincidence, centered on the MISR block that contains the MISR-SeaBASS coincidence. We then interpolate the MODIS-Terra *Chl* data, as well as the associated MODIS flags, to the MISR grid via nearest-neighbor interpolation. ~~We~~In an attempt to ensure the highest quality retrieval possible, we flag all MISR/MODIS data based on the following ~~conditions~~criteria:

- Any MISR/MODIS data where the MODIS *Chl* flag data is masked (at level 3) according to ~~https://oceancolor.gsfc.nasa.gov/ems/atbd/ocl2flags/~~https://oceancolor.gsfc.nasa.gov/ems/atbd/ocl2flags/.
- Any MISR/MODIS data where the MISR aerosol retrieval acceptance criterion is violated. In this case the criterion, $\chi^2 > 1.0$, is calculated over the all four wavelengths for all glint-free cameras (see section 2.1 above). This should help prevent poor aerosol retrievals impacting the MISR *Chl* retrieval.
- Any MISR/MODIS data where MISR 446nm AOD > 1.0 . AOD above this value over ocean tends to occur only in cases of dust, smoke, or pollution plumes, or unmasked clouds. As the surface signal is very small for these cases, especially for the off-nadir cameras, MISR should have little or no sensitivity to *Chl* in these situations.
- Any MISR/MODIS data where the MISR *Chl* $\chi^2 > 1.0$, calculated over the over the blue and green “A” and “B” glint-free cameras, as these cameras contain the most information about the surface.
- Any MISR/MODIS data where *in situ Chl* > 4.510 mg m^{-3} , as our *Chl* model is not expected to work at all in this regime.

For comparisons with SeaBASS, we average (in \log_{10} space) up to 5×5 MISR 1.1 km /MODIS 1 km *Chl* retrievals centered on the SeaBASS location, and compare each of the MISR and MODIS-Terra *Chl* to the corresponding SeaBASS value. ~~We also average together the MISR and MODIS results over the same locations.~~ Following conventional practice, \log_{10} of the MISR, MODIS, and SeaBASS *Chl* data is taken before any statistics are computed, except the mean relative error (MRE).

4.3.1 Validation against SeaBASS

Figure 6.3 shows ~~three sets of~~ scatterplots for MISR, and MODIS-Terra, ~~and the mean of MISR and MODIS, all~~ retrieved *Chl* vs. SeaBASS coincident *in situ Chl*. Points left of the black vertical line in Figure 6.3 and Table 2.1 demonstrate MISR sensitivity to retrieving Chlorophyll-a when the *in situ* value is less than 1.5 mg m^{-3} . ~~Statistics for $Chl_{in\text{-}situ} \leq 10$ in Table 2 are shown for completeness. Referring to Table 2, which represents an upper bound on where we expect good-quality results. Statistics for $Chl_{in\text{-}situ} \leq 10$ in Table 1 are shown for completeness. Compared to SeaBASS, for *in situ Chl* values $< 1.5 \text{ mg m}^{-3}$, MISR reports a correlation coefficient (r) of 0.86, a median absolute error (MAE) of 0.10, root-mean-squared error (RMSE) of 0.25, and MRE of 0.52. We also performed three sets of the two-sample Kolmogorov-Smirnov test to compare whether these MISR, MODIS, and SeaBASS populations are distinguishable. The null hypothesis that the MISR and MODIS~~

datasets are taken from the same distribution cannot be rejected ($p=0.96$), likely a result of having too few data points and/or strong co-variance. Not surprisingly, statistics for the 49 SeaBASS coincidences that meet our criteria indicate that the MISR RA performs almost as well as MODIS Terra for these cases. Formally, the average of MISR and MODIS (in \log_{10} -space) produce the best overall agreement with SeaBASS: MAE decreases by 29% as compared to MODIS alone, RMSE decreases by 5%, MRE decreases by 17%, and r remains unchanged. However, given P-values of 0.25 and 0.37 also indicate that although the MISR and MODIS *Chl* data (respectively) are not statistically distinguishable from SeaBASS, they appear more similar to each other than they are to SeaBASS. Given the small sample size, it is not possible to draw strong conclusions about whether MISR could in general add value to the MODIS Terra Ocean color product in regions where MODIS-Terra reports *Chl*, despite the likelihood that MISR aerosol retrieval constraints would produce a more accurate atmospheric correction. However, MISR can add value in the glint-contaminated portion of the MODIS-Terra orbit, and probably in regions of medium-high aerosol loading (both of which are shown subsequently), where aerosol-type information could improve surface retrieval results (e.g., Kahn et al., 2016).

4.3.2 Comparison against MODIS-Terra

Because the SeaBASS validation dataset contains very few matchups with MISR, in part due to the relatively narrow MISR swath, we compare MISR 1.1 km *Chl* retrievals with collocated MODIS 1 km *Chl* retrievals over much larger regions surrounding the MISR-SeaBASS coincidence locations, using the method described above. We compare to MODIS-Terra for this regional-context exercise due to the assessments already performed on these the MODIS *Chl* data with the much larger number of MODIS-SeaBASS coincidences (e.g., Franz et al., 2012). As such, we compare the MISR RA *Chl* data with all valid pixels for which MODIS *Chl* ≤ 10 mg m⁻³.

Figure 74 shows comparisons between the MISR RA and MODIS-retrieved *Chl*, for MODIS *Chl* ≤ 10.0 mg m⁻³. The black vertical line indicates 1.5 mg m⁻³. Statistics for the MISR MODIS *Chl* comparisons, as a function of MISR retrieved AOD, are summarized in Table 3. Overall, Figure 7 and Table 3 indicate that the agreement between MISR and MODIS is much better than the agreement between either MISR or MODIS and SeaBASS, as we expect higher-quality MISR *Chl* retrievals to the left of this line. The agreement between MISR and MODIS is especially good up until about MISR-retrieved *Chl* values of 0.5 mg m⁻³. For MISR *Chl* between 0.5 and 3.0 mg m⁻³, Figure 74 indicates that a scale factor could be applied to the MISR data to bring the data into better agreement with MODIS (and likely SeaBASS as well). Statistics for the MISR-MODIS *Chl* comparisons, as a function of MODIS-retrieved *Chl*, are summarized in Table 2. Comparing MISR vs. MODIS for MODIS *Chl* ≤ 1.5 : r is 0.05 higher than MODIS vs. SeaBASS, Mean Absolute Error is 36% lower million data points with MODIS *Chl* < 1.5 mg m⁻³: $r=0.96$, MAE=0.09, RMSE is 32% lower=0.15, and MRE is 57% lower. This suggests one or more of the following: (1) MISR-MODIS *Chl* errors co-vary (which is probable to some degree), (2) *Chl* variability is important on =0.23. A two-sample Kolmogorov-Smirnov test comparing these temporal/spatial scales, or (3) we need more *in situ* data two datasets demonstrates that they are statistically different ($p < 0.001$). Overall, although Figure 4 and Table 2 indicate that the agreement between MISR and MODIS appears to obtain robust statistics, be much better than the agreement between either MISR or MODIS and SeaBASS (Figure 3 and Table 1), it is possible that this is an artifact of a small MISR-SeaBASS sample size. However, comparisons between MODIS-Terra, SeaWIFS, and SeaBASS on the SeaBASS website suggest that this behavior is real, as SeaWIFS and MODIS-Terra agree much better with each other than with SeaBASS

Formatted: Heading 2, Right: 0 cm

Formatted: Font: Not Bold

Formatted: Right: 0 cm

<https://seabass.gsfc.nasa.gov/search#bio>). This strongly suggests that satellite remote-sensing co-variation is playing a substantial role in the comparisons between MISR, MODIS and SeaBASS. Interestingly, SeaWIFS also agrees better with MODIS-Terra than MISR does. Regardless, Figures 63 and 74 indicate that there is skill in the MISR Chl retrieval, which could be exploited.

Formatted: Font: Not Italic

Formatted: Font: Not Bold

4. Example MISR Aerosol-Surface Retrievals Over Ocean

We present here two examples of individual MISR RA joint surface and atmosphere retrievals, and comparisons with the corresponding MISR SA retrievals, MODIS Chl results, and embedded AERONET AOD measurements and particle property retrievals. Figure 5 presents both the SA and RA aerosol retrievals, along with the MISR RA and MODIS Chl results for a region of the Atlantic along the east coast of the US that includes the Chesapeake Bay and two coastal AERONET sites, in August 2003. Weakly to non-absorbing, relatively small, pollution particles are expected in this region and season, as confirmed by the AERONET inversion results. Both the SA (Diner et al., 2008; Kahn et al., 2010) and RA also identify the scene as dominated by small, spherical particles. Although the RA finds weakly or non-absorbing particles spread fairly uniformly over the entire scene, the SA appears to incorrectly identify part of the scene as contaminated by moderately absorbing aerosol. The MISR SA best estimate aerosol mixture preferentially selects lower SSA (Figure 5, ~ 0.91) aerosol mixtures near the coast, where both MODIS and the MISR RA report elevated Chl. In this same region, AERONET and MISR RA find that SSA falls within the range of 0.98 to 1.0. For particle size, represented here by ANG, the MISR RA tends to pick slightly larger aerosol models (ANG ~ 1.72), in poorer agreement with AERONET (ANG ~ 2.05) than the SA (ANG ~ 2.00). This is probably related to the aerosol optical model options in the RA (e.g., Limbacher and Kahn, 2014), which are being reconsidered as part of continuing work. Ultimately, we are hoping to systematically acquire direct, *in situ* measurements of the particle optical and chemical properties for the major aerosol air mass types, to put these remote-sensing algorithm assumptions on more solid footing [Kahn et al., 2016]. Note also that the MISR Chl results compare very well with the corresponding MODIS values where coincident retrievals were obtained, and here the multi-angle data offer an advantage, as the MODIS camera is in sun-glint over the eastern half of the scene, whereas the MISR off-nadir cameras make it possible to perform Chl and aerosol retrievals over the entire area.

Figure

Formatted: Font: Not Bold

6 captures a scene in the mid-south Atlantic Ocean near Ascension Island, where smoke advected from southern Africa is commonly found. Both the SA and RA identify much of the scene as dominated by small, spherical absorbing aerosol, consistent with both the Ascension Island AERONET station and expectation. The scene is covered in broken cloud, typical of much of this ocean region, which makes aerosol remote-sensing retrievals especially challenging. Both the SA and the RA results exhibit 3-d light-scattering effects near cloud edges. Here difference between the SA and RA retrieval-region sizes has significant consequences: the SA appears to have more coverage, whereas the cloud-edge anomalies are more localized in the higher-resolution RA retrievals, and the SA shows substantially more SSA (and hence retrieved aerosol type) variability (0.92 ± 0.08) compared to the RA (0.91 ± 0.04). The variability artifacts due to 3-d effects also show up in the ANG and Fr. Non-Sph for both the SA and RA, and are reflected in the MISR RA retrieved Chl, giving an indication of the impact aerosol type has on retrieved ocean color.

5. Conclusions

In Limbacher and Kahn (2014), we detailed extensive modifications to the MISR Research Aerosol retrieval algorithm (RA) that reduced the 0.024 AOD high bias for $AOD_{558nm} < 0.10$ to ~ 0.01 or less. The modifications also improved the results of the RA in general, compared to a set of about 1,100 coincidences with ground-truth observations (lower RMSE, etc.). In from coincident AERONET sun photometer observations. We also found that the success of MISR aerosol retrieval algorithm refinements depends in part on the accuracy of instrument radiometric calibration. So, in Limbacher and Kahn (2015), we implemented a stray-light correction for the near-nadir cameras based on empirical image analysis with MODIS that. This further reduced the remaining high bias at low AOD and also improved statistical comparisons to the validation data overall. Here, we introduce a coupled surface component to the RA over water. More accurately accounting for ocean surface contributions to TOA reflectance should improve aerosol-type retrievals (which will be explored in part II of this paper). As part of the MISR calibration refinement effort, we also performed a radiometric trend analysis over three stable, relatively homogeneous desert sites to identify and quantify radiometric drift in each of the 36 MISR channels. We then applied the radiometric drift corrections to the MISR data in general, further refined the stray light corrections for the nadir viewing camera, and applied the stray light corrections to the other cameras. Finally, we revised the MISR retrieval algorithm to include a chlorophyll a retrieval, which is implemented so results can be derived from single or multiple MISR cameras temporal radiometric drift in each of the 36 MISR channels.

Justification for the new corrections is as follows: The radiometric trend analysis shows consistent, decreasing BRFs over time for three stable desert sites that can easily be corrected. Errors due to stray light in the MISR were formally addressed in Limbacher and Kahn [2015], and the adjustments we make in this paper to our ghosting model better represent the stray light observed in MISR MODIS comparisons. These adjustments also allow the corrections to be performed as a series of convolutions, which substantially reduces the ghosting correction implementation time compared to the approach in Limbacher and Kahn [2015]. However, the corrections would run even faster and require fewer approximations if performed earlier in the MISR data stream, at L1B1, rather than with the L1B2 data available to us, i.e., prior to data rotation, de-convolution, and trimming near the poles.

Validation of the MISR RA-retrieved *Chl*, with all radiometric corrections applied, was performed in part by comparison with coincident SeaBASS *in-situ* observations. Additionally, further comparisons were made against the previously validated MODIS-Terra ocean color *Chl* retrievals, because of the relatively small MISR-SeaBASS coincident dataset. Results show that the MISR RA can retrieve *Chl* reliably if the MODIS-reported $Chl \leq 1.5 \text{ mg m}^{-3}$, which represents a large fraction of the Earth's ocean area (Figure 4). Compared to SeaBASS, for *in-situ* *Chl* values $\leq 1.5 \text{ mg m}^{-3}$, MISR (MODIS) reports a correlation coefficient of 0.86 (0.91), MAE is 0.10 (0.14), RMSE is 0.25 (0.22), and MRE is 0.52 (0.54), indicating. A comparison of the 49 coincident MISR agrees with MODIS, and SeaBASS nearly as well as MODIS Terra when *in-situ* $Chl \leq 1.5$, though for only the 49 available coincidences observations (Figure 3), using three two-sample Kolmogorov-Smirnov tests, indicates that it is not possible to distinguish statistically between any of these three small *Chl* data sets. For the larger ($n=1,499,610$) MISR-MODIS dataset with MODIS-retrieved $Chl \leq 1.5 \text{ mg m}^{-3}$, we find $r=0.96$, $MAE=0.09$, $RMSE=0.15$, and $MRE=0.23$, indicating that the agreement between MISR and MODIS is substantially better

Formatted: Font: Not Bold

Formatted: Tab stops: 16.51 cm,

Formatted: Font: 12 pt

Formatted: Heading 1, Right: 0 cm, Space Before: 12 pt

Formatted: Font: 12 pt, Not Bold

Formatted: Right: 0 cm

Formatted: Font: Not Italic

Formatted: Font: Not Italic

Formatted: Right: 0 cm

Formatted: Font: Italic

Formatted: Font: Italic

~~than the agreement between either instrument and SeaBASS. Differences between these statistics could be explained by one or more of three factors: (1) the number of MISR-SeaBASS coincidences is too small to reach robust conclusions, (2) the temporal/spatial variability of chlorophyll a is substantial for the 3 hours or the 5x5 box over which the comparisons are made, or (3) the errors in MISR and MODIS Terra retrieved *Chl* co vary.~~ Although ~~we find that~~ the MISR RA as implemented here lacks much sensitivity to retrieved *Chl* above 1.5 ~~mg m⁻³~~, and especially above about 3 mg m⁻³, this result was anticipated, due to the lack of spectral bands between 446 and 558 nm ~~(Diner et al, 1998).~~ However, with further work, adjustments to the scattering and absorption terms in Equation (1) might improve the results in the higher *Chl* regime, particularly if MODIS-Terra reflectances can be integrated into the algorithm.

Formatted: Font: Times New Roman, Font color: Auto

Formatted: Font: Not Italic

Obtaining MISR *Chl* retrievals can help fill in the glint-contaminated regions in the single-view MODIS-Terra swath near the solar equator. ~~as only a few of MISR's nine view angles will be contaminated by glint in any one location, allowing the others to be used for the aerosol/*Chl* retrieval.~~ In addition, these MISR *Chl* results are derived self-consistently with aerosol amount and type in a physical retrieval, which from the ocean color perspective provides a more robust "atmospheric correction" for the surface retrieval. This work formally opens the door for the use of MISR data in ocean color, complementing the better-constrained and more extensive spectral coverage of MODIS ocean color retrievals. With the improved ocean-surface boundary condition, the MISR multi-angular data should also allow for better-constrained aerosol products, particularly non-sphericity and single-scattering albedo. ~~A few detailed examples of individual RA joint surface and atmosphere retrievals are given in the Supplemental Material.~~ In the future, it might be possible to ingest collocated MISR and MODIS-Terra reflectances, and use the strengths of each instrument in a complimentary manner.

Formatted: Font: 10 pt

Formatted: Heading 1, Right: 0 cm

Acknowledgments

We thank Chris Proctor and NASA's Ocean Biology Processing Group for providing the MODIS Terra Ocean Color products and the SeaBASS group (and cruise PIs) for compiling and providing their in-situ ocean color data sets. We thank our colleagues on the Jet Propulsion Laboratory's MISR instrument team and at the NASA Langley Research Center's Atmospheric Sciences Data Center for their roles in producing the MISR Standard data sets, and Brent Holben at NASA Goddard and the AERONET team for producing and maintaining this critical validation dataset. We also thank Carol Bruegge, Sergey Korin and Andrew Sayer for *many* helpful discussions, Alexei Lyapustin for providing ~~his~~ MODIS ~~radiometric correction~~ code, as well as Andrew Sayer, James Butler, and Carol Bruegge for comments on an early version of the manuscript. This research is supported in part by NASA's Climate and Radiation Research and Analysis Program under H. Maring, and NASA's Atmospheric Composition Program under R. Eckman.

Formatted: Right: 0 cm

Appendix A. MISR Radiometric Calibration Adjustments

As mentioned in the introduction, instrument calibration can affect retrieval products such as AOD, aerosol type, and ocean surface properties (Limbacher and Kahn, 2015). Calibration includes determination of (1) the absolute radiometric scale, as well as (2) the relative band-to-band response among the four MISR spectral bands, (3) camera-to-camera response among

the nine MISR cameras, (4) flat-fielding across the MISR imagery (i.e., CCD detector-based gain errors, which show up as cross-track biases in reflectance), and (5) temporal trends in these quantities. Considerable effort has been expended to assess MISR radiometric calibration and to meet the standards of approximately 3% absolute and 1% channel-to-channel, established pre-launch. Previous work involved pre-launch laboratory studies (Bruegge et al., 1999), on-board-calibrator analysis and lunar calibration, along with vicarious calibration over bright land targets (Bruegge et al., 2004; 2007; 2014), symmetry tests comparing the forward and aft-viewing cameras across the solar equator (Diner et al., 2004), and over-ocean dark target vicarious calibration (Kahn et al., 2005). Cross-calibration analysis has been performed over bright and dark land and ocean surfaces with the MODerate-resolution Imaging Spectroradiometer (MODIS), that flies aboard the Terra satellite with MISR (Lyapustin et al., 2007), and MODIS combined with the MEdium Resolution Imaging Spectrometer (MERIS), the airborne AirMISR instrument, the LandSat-7 ETM+ (Bruegge et al., 2007), and the Polarization and Directionality of the Earth's Reflectances-2 (POLDER-2) (Lallart et al., 2008). A synthesis of much of this work is given in Bruegge et al. (2014). Limbacher and Kahn (2015) used image analysis, including comparisons with coincident MODIS observations, to characterize flat-fielding errors, and to identify empirical relationships that correct anomalies exhibiting spatial structure in high-contrast scenes, an aggregate of “ghosting” light reflections (or stray-light) within the cameras. Here we make minor adjustments to our earlier ghosting and flat-fielding corrections. For the flat-fielding characterization, we select only low-contrast scenes, where ghosting artifacts are minimal, and we then normalize the mean MISR-MODIS ratios for the entire scene to unity. For the ghosting modifications, we normalize the MISR-MODIS ratios to an area of little contrast, where stray light is unlikely to be an issue. In the course of that analysis, we also observed systematic, temporal drifts in the measured reflectances, addressed in A.2 below.

Formatted: Font: Not Italic

A.1. TOA Reflectance Pre-processing and Stray-light Corrections

In the RA pre-processing, all MISR L1B2 reflectance data are first averaged to 1.1 km. The reflectances are then rotated to the L1B1 format, as described in Limbacher and Kahn (2015), and updated stray-light and flat-fielding corrections are applied before being rotated back to L1B2 format. Compared to Limbacher and Kahn (2015), we modify the stray-light corrections in the following way:

Formatted: Right: 0 cm

- The primary ghost term has been divided into a discrete ghosting component (reflected images of features in the scene) and an unstructured veiling-light component.
 - This revised primary ghost has a band-and-camera-dependent along-track offset applied, as indicated by MISR lunar observations acquired on 14 April 2003 (e.g., Bruegge et al., 2004).
 - The primary ghost image is also stretched/squeezed across-track (for the near-nadir “A” cameras only), based on further comparisons with MODIS Terra, following the same approach as our earlier work.
- Via ray tracing, it was found that the “secondary ghosting” term in Limbacher and Kahn (2015) distributes light uniformly from the left- or right-most ~1/3 of the scene to the remainder of that half of the scene (Ab Davis, personal communication, 2016), and the correction has been modified accordingly.
- All stray-light terms are now represented as convolutions, which are much quicker to compute than applying the functions pixel-by-pixel as was done in our earlier work.
- The magnitudes of all stray-light terms have been adjusted as a result of adding the unstructured veiling-light component.
- The stray-light model for the An camera (all four bands) is used for all off-nadir cameras. Only the along-track offset and primary ghost stretching are varied by camera.

Formatted: Indent: Hanging: 0.63 cm, Right: 0 cm

Formatted: Font: Not Italic

Formatted: Indent: Hanging: 0.63 cm, Right: 0 cm

We then correct for temporal degradation in the MISR calibration (see A.2. below) and revise the band-to-band calibration. We change the band-to-band calibration by increasing the red reflectance 0.75% and decreasing the near-infrared (NIR) reflectance 0.75%, adjustments that are within the calibration uncertainty and are required to match a global set of coincident, spectral aerosol optical depth validation data (Limbacher and Kahn, 2014; 2015). We also apply corrections to the radiance data to smooth out apparent anomalies in the instrument gain, based on Bruegge et al. (in preparation).

Formatted: Font: Not Italic

A.2. Temporal Trend Characterization and Correction

We characterize here temporal trends in the instrument calibration, again using an empirical image-analysis approach. Bruegge et al. (2014) identified temporal trends in the MISR bidirectional reflectance factor (BRF, computed as described in Step 1a. below) data, based on a time-series of mean BRFs for a region approximately 10×20 high-resolution (275 m) MISR pixels, a region roughly 2.5×6 km in size, centered at (27.21° N; 26.10° E) within the Egypt-1 desert site. Although this site is stable over time, we adopt a different methodology, similar to Lyapustin et al. (2014), but without performing an atmospheric correction (thus we assume no trend in TOA reflectance due to changes in AOD/aerosol type). The temporal trending analysis is done here based on BRFs averaged over larger areas, and at three stable desert sites (Egypt-1, Libya-1, and Libya-4). Compared to Bruegge et al. (2014), both techniques are valid, but we limit geo-location error by averaging, and we reduce the influence of clouds by selecting the median BRF pixel from each case.

Formatted: Font: Not Italic

Formatted: Font: Not Italic

The first challenge to performing the temporal-trend analysis is finding suitable homogeneous regions. The following was done to select study regions within each of the three sites: the spectral coefficients of variation (standard deviation divided by the mean) were calculated for rolling 50×50 pixel patches, in each spectral band of the nadir camera, for three or more orbits, and (b) the 50×50 pixel patch having the smallest maximum coefficient of variation among all four bands was chosen for subsequent time-series analysis. The central coordinates for the sites selected are: Egypt-1 (26.62° N, 26.18° E), Libya-1 (24.73° N, 13.52° E), and Libya-4 (28.77° N, 23.50° E). Information about these calibration sites can be found at http://calval.cr.usgs.gov/rst-resources/sites_catalog/radiometric-sites/test-site-gallery/.

Formatted: Right: 0 cm

The central coordinate of each study site is imaged repeatedly by MISR along at least two distinct paths having different sub-spacecraft ground tracks, and therefore different viewing geometries at the site. (A "path" is one of 233 ground tracks that the Terra satellite covers, repeatedly, every 16 days.) So the following procedure was applied separately to each path and camera (6 paths \times 9 cameras), for data acquired between January 1, 2002, and December 31, 2014, giving 13 full years of MISR data. (Prior to January 1 2002, the spacecraft equator-crossing time was not yet stable, so solar geometry varied too much for this time-series analysis.) All observations of each site, about four per month, were initially included. Note that we also apply flat-fielding corrections to the nadir camera (Limbacher and Kahn, 2015), and additional corrections to the radiance data in all cameras to smooth the instrument gain temporal samples (Carol Bruegge, personal communication, 2016). We characterize the temporal trends as follows:

Formatted: Right: 0 cm

5) Calculate median patch reflectance for each orbit

- a. Perform Earth-Sun and solar zenith normalization according to: $BRF=L*([\pi \times D^2] / [E(i) \times \cos(SZA)])$, where L is the top-of-atmosphere radiance, D is the sun-Earth distance in AU, E(i) is the band-weighted exo-atmospheric solar irradiance for band (i), and SZA is the solar zenith angle.

- b. Calculate the median (and mean) BRF and standard deviation over a region 25 km in radius surrounding the central latitude/longitude coordinate.
- c. If the wavelength-maximized coefficient of variation is less than 0.02, save the median BRF for use in the time series, otherwise discard the data.

Median BRF values for at least 193 orbits, and up to 229 orbits, were retained for all 6 paths, 4 spectral bands, and 9 cameras at this step.

6) Remove outliers for each path/site and spectral band

- a. Arrange the saved median BRFs by acquisition date, fit a line to the values, and subtract the linear trend from the data (to be added back after outliers are removed and the data are deseasonalized).
- b. Aggregate the data by day-of-year (DOY) and smooth the sorted, de-trended BRFs using a 21-point (i.e., ± 10 data point) rolling average. (The data are sufficiently dense that dividing each data point with the mean of 21 surrounding data points does not create significant artifacts in the time-series.) This removes the seasonality, but does not remove outliers from the data, therefore allowing us to identify them.

~~a-c.~~ Identify BRFs that fall outside 2σ from time series.

~~b-d.~~ Remove the identified outliers from the original data.

This step removed 3-14% of data outliers from each time-series.

7) De-seasonalize the data for each site and spectral band

- a. Fit a line to the original, time-ordered BRFs (for all 13 years), with outliers removed, and again linearly de-trend the data.
- b. Re-aggregate the data by DOY and divide the BRFs by their 21-point (± 10 data point) rolling average.
- ~~a-c.~~ Rearrange the data by time and add back the linear trend from Step 3a.

Step 3 is illustrated in Figure A1 for the Libya-4 site.

8) Normalize the data

- a. Normalize the data so the time-series mean for each spectral band at each site is 1.0, which retains the linear trends in each time-series, but allows data from multiple sites and paths to be compared.

The result is 216 normalized time-series, one for each MISR camera and band, for each of two paths at three sites.

- b. These time-series are then aggregated across all paths to produce 36-time series, one for each MISR channel (Figure A2).

The linear percent change per decade and its 95th percent confidence interval are then calculated for each channel, and the results are presented in Table 3 and Figure A3. The trends are all negative, as might be expected due to sensor degradation over time. They are smallest in the blue band for all but the forward-viewing 70.5° (Df) and 60.0° (Cf) cameras, smallest for the aft-viewing 70.5° (Da) and 60.0° (Ca) cameras for all bands except the NIR, and largest for the An, and 26.1° forward (Af) and aft-viewing (Aa) cameras. The largest drift overall is about -1.5% per decade for the An camera red and NIR bands, and the uncertainty in these results ranges from ~0.1 % per decade to ~0.4 % per decade, depending on wavelength and camera. The apparent stability of the MISR blue band is probably due to the use of the blue diode to assess degradation of the MISR on-board calibration panels (Bruegge et al., 2007). Because MISR calibration assumes that the panel degrades in a spectrally invariant way (likely a poor assumption), this subsequently results in a spectral variant TOA reflectance drift with time.

Formatted: Right: 0 cm

Formatted: Right: 0 cm

Formatted: Right: 0 cm

Formatted: Right: 0 cm

References

Atlas, R., R. N. Hoffman, J. Ardizzone, S. M. Leidner, J. C. Jusem, D. K. Smith, D. Gombos, 2011. A cross-calibrated, multiplatform ocean surface wind velocity product for meteorological and oceanographic applications. *Bull. Amer. Meteor. Soc.*, 92, 157-174, doi: 10.1175/2010BAMS2946.1

Bailey, S.W. and P.J. Werdell, 2006. A multi-sensor approach for the on-orbit validation of ocean color satellite data products, *Rem. Sens. Environ.* **102**, 12-23.

Barrot, G., Mangin, A., and Pinnock, S., 2010. GlobColour Product User Guide, <http://www.globcolour.info>, accessed: 31 January 2014.

Behrenfeld, M.J., R.T. O'Malley, D.A. Siegel, C.R. McClain, J.L. Sarmiento, G.C. Feldman, A.J. Milligan, P.G. Falkowski, R. M. Letelier, and E.S. Boss, 2006. Climate-driven trends in contemporary ocean productivity. *Nature* 444, 752-755.

Bruegge, C.J., D.J. Diner, R.P. Korechoff, and M. Lee, 1999. MISR Level 1 Radiance Scaling and Conditioning Algorithm Theoretical Basis. Jet Propulsion Laboratory JPL D-11507, Rev E. From: <http://eosps0.gsfc.nasa.gov/sites/default/files/atbd/atbd-misr-02.pdf>

Bruegge, C.J., W.A. Abdou, D.J. Diner, B.J. Gaitley, M.C. Helmlinger, R.A. Kahn, and J.V. Martonchik, 2004. Validating the MISR radiometric scale for the ocean aerosol science communities. In: Post-launch calibration of satellite sensors, Stanley A. Morain and Amelia M. Budge, editors. A.A. Balkema Publishers, Leiden, Netherlands, pp.103-115.

Bruegge, C.J., D.J. Diner, R.A. Kahn, N. Chrien, M.C. Helmlinger, B.J. Gaitley, W.A. Abdou, 2007. The MISR radiometric calibration process, *Remt. Sensing Environ.* 107, 2-11, doi:10.1016/j.rse.2006.07.024.

Bruegge, C.J., D.J. Diner, E. Gray, V. Jovanovic, E. Gray, L. Di Girolamo, and G. Zhao, 2014. Radiometric stability of the Multi-angle Imaging SpectroRadiometer (MISR) following 15 years on-orbit. *Proc. SPIE V.* 9218, doi: 10.1118/12.2062319.

Chrien, N. L., C. J. Bruegge, and B. J. Gaitley, 2001. AirMISR laboratory calibration and in-flight performance results. *Remt. Sens. Environ.* **77**, 328-337.

Chen, C., P. Shi, and H. Zhan, 2003. A local algorithm for estimation of yellow substance (gelbstoff) in coastal waters from SeaWiFS data: Pearl River estuary, China, *International Journal of Remote Sensing* **24** (5), doi: 10.1080/0143116021000047901

Formatted: Font: Times New Roman, 12 pt

Formatted: Font: Times New Roman, 12 pt, Not Bold

Formatted: Heading 1, Right: 0 cm

Formatted: Font: Times New Roman, German (Germany)

Formatted: Font: Times New Roman

Formatted: Right: 0 cm, Space Before: 0 pt

Formatted: German (Germany)

Formatted: Font: Times New Roman, German (Germany)

Formatted: Font: Times New Roman, Not Italic

Formatted: Font: Times New Roman

Formatted: Right: 0 cm, Tab stops: Not at 17.62 cm

Formatted: Font: Times New Roman, Not Italic

Formatted: Font: Times New Roman

Formatted: Font: Times New Roman

Formatted: Right: 0 cm, Space Before: 0 pt

Formatted: Font: Times New Roman

Formatted: Right: 0 cm, Space Before: 0 pt

Formatted: Font: Times New Roman, Not Italic

Formatted: Font: Times New Roman

Formatted: Font: Times New Roman

Formatted: Right: 0 cm, Space Before: 0 pt

Formatted: Font: Times New Roman

Formatted: Hyperlink, Font: Times New Roman

Formatted: Font: Times New Roman

Formatted: Right: 0 cm

Formatted: Font: Times New Roman, Not Italic

Formatted: Font: Times New Roman

Formatted: Font: Times New Roman, Not Italic

Formatted: Font: Times New Roman

Formatted: Font: Times New Roman, Not Italic

Formatted: Font: Times New Roman

Devred, E., S. Sathyendranath, V. Stuart, H. Maass, O. Ulloa, and T. Platt, 2006. A two-component model of phytoplankton absorption in the open ocean: Theory and applications, *J. Geophys. Res.*, 111, C03011, doi:[10.1029/2005JC002880](https://doi.org/10.1029/2005JC002880)

Diner, D. J., et al., 1998. Multi-angle Imaging SpectroRadiometer (MISR) instrument description and experiment overview, in *IEEE Transactions on Geoscience and Remote Sensing*, vol. 36, no. 4, pp. 1072-1087, Jul 1998. doi: 10.1109/36.700992

Diner, D.J., R.A. Kahn, C.J. Bruegge, J.V. Martonchik, W.A. Abdou, B.J. Gaitley, M.C. Helmlinger, O.V. Kalashnikova, and W-H. Li, 2004. Refinements to MISR's radiometric calibration and implications for establishing a climate-quality aerosol observing system. *Proc. of SPIE Vol. 5652*, 57-65.

Diner, D. J., et al. 2008. Multi-Angle Imaging SpectroRadiometer Level 2 Aerosol Retrieval Algorithm Theoretical Basis, Revision G, JPL D-11400, Jet Propulsion Laboratory, California Institute of Technology, Pasadena.

~~Draxler, R. R. and Rolph G. D. 2003. HYSPLIT (HYbrid Single Particle Lagrangian Integrated Trajectory) Model access via the NOAA ARL READY Website, NOAA Air Resour. Lab., Silver Spring, Md. available at: <http://www.arl.noaa.gov/ready/hysplit4.html>.~~

Dubovik, O. and M. D. King, 2000: A flexible inversion algorithm for retrieval of aerosol optical properties from Sun and sky radiance measurements, *J. Geophys. Res.*, 105, 20 673-20 696.

Dubovik, O., A. Sinyuk, T. Lapyonok, B. N. Holben, M. Mishchenko, P. Yang, T. F. Eck, H. Volten, O. Munoz, B. Veihelmann, W. J. van der Zande, J-F Leon, M. Sorokin, and I. Slutsker, 2006. Application of spheroid models to account for aerosol particle nonsphericity in remote sensing of desert dust. *J. Geophys. Res.*, 111, doi:[10.1029/2005JD006619](https://doi.org/10.1029/2005JD006619)

Eck, T. F., Holben, B. N., Reid, J. S., Dubovik, O., Smirnov, A., O'Neill, N. T., Slutsker, I., and Kinne, S., 1999. Wavelength dependence of the optical depth of biomass burning, urban, and desert dust aerosols, *J. Geophys. Res.*, 104, 31333-31349, doi:10.1029/1999JD900923, 1999.

Franz, B.A., S.W. Bailey, G. Meister, and P.J. Werdell, 2012. Consistency of the NASA Ocean Color Data Record. *Proc. Ocean Optics 2012*, Glasgow, Scotland, 8-12 October 2012.

Gordon, H.R. and Wang, M., 1994. Retrieval of water-leaving radiance and aerosol optical thickness over oceans with SeaWiFS: a preliminary algorithm. *Appl. Opt.* 33, 443-452.

Heukelem, L. V., Thomas, C. S., and P. M. Glibert, 2002. Sources Of Variability In Chlorophyll Analysis By Fluorometry And High Performance Liquid Chromatography In a SIMBIOS Inter-Calibration Exercise. *NASA TM 2002-02338-0*, May 2002.

Formatted: Font: Times New Roman

Formatted: Font: Times New Roman

Formatted: Font: Times New Roman, Not Italic

Formatted: Font: Times New Roman

Formatted: Font: Times New Roman, Not Italic

Formatted: Font: Times New Roman

Formatted: Default Paragraph Font, Font: Times New Roman

Field Code Changed

Formatted: HTML Cite, Font: Times New Roman

Formatted: Font: Times New Roman

Formatted: Font: Times New Roman

Formatted: Font: Times New Roman, Not Italic

Formatted: Font: Times New Roman

Formatted: Right: 0 cm, Add space between paragraphs of the same style, Line spacing: single

Formatted: Font: Times New Roman

Formatted: Font: Times New Roman

Formatted: Normal, Left, Right: 0

Formatted: Font: 10 pt

Formatted: Font: 10 pt, Not Italic

Formatted: Font: 10 pt

Formatted: Font: 10 pt

Formatted: Normal, Left, Right: 0

Formatted: Font: 10 pt

Formatted: Font: 10 pt

Formatted: Font: 10 pt

Formatted: Hyperlink

Formatted: Font: Times New Roman

Formatted: Right: 0 cm

Formatted: Font: Times New Roman

Formatted: Font: Times New Roman, Not Italic

Formatted: Font: Times New Roman

Formatted: Font: Times New Roman

Formatted: Right: 0 cm, Tab stops: Not at 16.51 cm

Formatted: Widow/Orphan control, Adjust space between Latin and Asian text, Adjust space between Asian text and numbers

Formatted: Font: Times New Roman

Formatted: Font: Times New Roman

Formatted: Right: 0 cm, Tab stops: Not at 16.51 cm

Holben, B. N., Eck, T. F., Slutsker, I., Tanre, D., Buis, J. P., Sezter, A., Vermote, E., Reagan, J. A., Kaufman, Y. J., Nakajima, T., Lavenu, F., Jankowiak, I., and Smirnov, A., 1998, AERONET – a federated instrument network and data archive for aerosol characterization, *Remote Sens. Environ.*, 66, 1–16, 1998.

Formatted: Right: 0 cm

Formatted: Font: Times New Roman

Formatted: Font: Times New Roman

Holben, B. N. et al., AERONET's Version 2.0 quality assurance criteria. Accessed 8-26-2016. http://aeronet.gsfc.nasa.gov/new_web/Documents/AERONETcriteria_final1.pdf

Formatted: Font: Times New Roman

Hu, C., Z. Lee, and B. Franz, 2012. Chlorophyll-a algorithms for oligotrophic oceans: A novel approach based on three-band reflectance difference, *J. Geophys. Res.*, 117, C01011, doi:10.1029/2011JC007395.

Formatted: Right: 0 cm, Tab stops: Not at 16.51 cm

Formatted: Right: 0 cm

~~Jovanovic, V.M., S.A. Lewicki, M.M. Smyth, J. Zong, and R.P. Korechhoff, 1999. MISR Level 1 Georectification and Registration Algorithm Theoretical Basis. Jet Propulsion Laboratory JPL D-11532, Rev. D. From: http://eosps.gsfc.nasa.gov/sites/default/files/atbd/atbd_misr_03.pdf~~

~~Jovanovic, V.M., M.A. Bull, M.M. Smyth, and J. Zong, 2002. MISR In-flight camera geometric model calibration and georectification performance. *IEEE Transact. Geosci. Remt. Sens.* 40, 1512-1519.~~

~~Kahn, R.A., A. M. Sayer, Z. Ahmad, and B. Franz, 2016. How Aerosol Amount and Type Affect SeaWiFS Ocean Color Retrievals. *J. Atm. Ocean Tech.* 23:6, 1185-1200, doi: 10.1175/JTECH-D-15-0121.1~~

Formatted: Font: Times New Roman

Formatted: Right: 0 cm

Formatted: Font: Times New Roman

Kahn, R., W-H. Li, J. Martonchik, C. Bruegge, D. Diner, B. Gaitley, W. Abdou, O. Dubovik, B. Holben, S. Smirnov, Z. Jin, and D. Clark, 2005. MISR low-light-level calibration, and implications for aerosol retrieval over dark water, *J. Atmosph. Sci.* 62, 1032-1062.

~~Kahn, R.A., P. Banerjee, and D. McDonald, 2001. The Sensitivity of Multiangle Imaging to Natural Mixtures of Aerosols Over Ocean, *J. Geophys. Res.* 106, 18219-18238.~~

~~Kahn, R.A., B.J. Gaitley, M.J. Garay, D.J. Diner, T. Eck, A. Smirnov, and B.N. Holben, 2010. Multiangle Imaging SpectroRadiometer global aerosol product assessment by comparison with the Aerosol Robotic Network. *J. Geophys. Res.* 115, D23209, doi: 10.1029/2010JD014601.~~

Formatted: Right: 0 cm

Formatted: Font: Times New Roman

~~Kahn, R.A., and J.A. Limbacher, 2012. Eyjafjalljökull Volcano Plume Particle Type Characterization from Space-Based Multi-angle Imaging. *Atmosph. Chem. Phys.* 12, 9459-9477, doi:10.5194/acp-12-9459-2012.~~

Kahn, R. A., and B. J. Gaitley, 2015. An analysis of global aerosol type as retrieved by MISR. *J. Geophys. Res. Atmos.* 120, doi:10.1002/2015JD023322.

Formatted: Font: Times New Roman

Formatted: Right: 0 cm

~~Kalashnikova, O. V., R. Kahn, I. N. Sokolik, and W. H. Li, 2005. Ability of multiangle remote sensing observations to identify and distinguish mineral dust types: Optical models and retrievals of optically thick plumes, *J. Geophys. Res.*, 110, D18S14, doi:10.1029/2004JD004550.~~

~~Kalashnikova, O. V., Garay, M. J., Martonehik, J. V., and Diner, D. J.: MISR Dark Water aerosol retrievals: operational algorithm sensitivity to particle non sphericity, *Atmos. Meas. Tech.*, 6, 2131–2154, doi:10.5194/amt-6-2131-2013, 2013.~~

~~Kahn, R.A., A. M. Sayer, Z. Ahmad, and B. Franz, 2016. How Aerosol Amount and Type Affect SeaWiFS Ocean Color Retrievals. *J. Atm. Ocean Tech.* 33:6, 1185-1209, doi: 10.1175/JTECH-D-15-0121.1~~

Lallart, P., R.A. Kahn, and D. Tanré, 2008. POLDER2/ADEOSII, MISR, and MODIS/Terra reflectance comparisons, *J. Geophys. Res.*, 113, D14S02, doi:10.1029/2007JD009656.

Lee, Z., J. Wei, K. Voss, M. Lewis, A. Bricaud, and Y. Huot, ~~2015.~~ Hyperspectral absorption coefficient of “pure” seawater in the range of 350–550 nm inverted from remote sensing reflectance. *Appl. Opt.* 54, 546-558 (2015).

~~Levy, R.C., S. Mattoo, L.A. Munchak, L.A. Remer, A.M. Sayer, F. Patadia, and N.C. Hsu, 2013. The Collection 6 MODIS aerosol products over land and ocean. *Atmos. Meas. Tech.* 6, 2989–3034, doi:10.5194/amt-6-2989-2013.~~

Limbacher, J.A., and R.A. Kahn, 2014. MISR Research-Aerosol-Algorithm Refinements For Dark Water Retrievals. *Atm. Meas. Tech.* 7, 1-19, doi:10.5194/amt-7-1-2014.

Limbacher, J. A. and R.A. Kahn, 2015. MISR empirical stray light corrections in high-contrast scenes. *Atm. Meas. Tech.*, 8, 2927-2943, doi:10.5194/amt-8-2927-2015.

Lyapustin, A., Y. Wang, R. Kahn, J. Xiong, A. Ignatov, R. Wolfe, A. Wu, B. Holben, C. Bruegge, 2007. Analysis of MODIS-MISR calibration differences using surface albedo around AERONET sites and cloud reflectance, *Remt. Sensing Environ.* 107, 12-21, doi:10.1016/j.rse.2006.09.028.

Lyapustin, A., Y. Wang, X. Xiong, G. Meister, S. Platnick, R. Levy, B. Franz, S. Korkin, T. Hilker, J. Tucker, F. Hall, P. Sellers, A. Wu, and A. Angal, 2014. Science impact of MODIS C5 calibration degradation and C6+ improvements. *Atmos. Meas. Tech. Discuss.*, 7, 7281–7319.

Martonehik, J.V., R.A. Kahn, and D.J. Diner, 2009. Retrieval of Aerosol Properties over Land Using MISR Observations. In: Kokhanovsky, A., ed., *Satellite Aerosol Remote Sensing Over Land*. Springer, Berlin.

~~Morel, A. and L. Prieur, 1977. Analysis of variations in ocean color. *J. Limnology and Oceanography*, 22, 709–722.~~

~~Morel, A., 1988. Optical modeling of the upper ocean in relation to its biogenous matter content (case I waters). *J. Geophys. Res.*, 93(C9), 10749–10768, doi:10.1029/JC093iC09p10749.~~

Formatted: Font: Times New Roman

Formatted: Right: 0 cm

Formatted: Font: Times New Roman

Formatted: Font: Times New Roman, Not Italic

Formatted: Font: Times New Roman

Formatted: Right: 0 cm

Formatted: Font: Times New Roman, Not Italic

Formatted: Font: Times New Roman

Formatted: Right: 0 cm, Tab stops: Not at 16.51 cm

Formatted: Right: 0 cm

Formatted: Font: Times New Roman, Not Italic

Formatted: Font: Times New Roman

Formatted: Right: 0 cm, Tab stops: Not at 1.62 cm + 3.23 cm + 4.85 cm + 6.46 cm + 8.08 cm + 9.69 cm + 11.31 cm + 12.92 cm + 14.54 cm + 19.39 cm + 21 cm + 22.62 cm + 24.23 cm + 25.85 cm

Formatted: Default Paragraph Font, Font: Times New Roman

Formatted: Font: Times New Roman

Formatted: Font: Times New Roman, Not Italic

Formatted: Right: 0 cm, Tab stops: Not at 1.62 cm + 3.23 cm + 4.85 cm + 6.46 cm + 8.08 cm + 9.69 cm + 11.31 cm + 12.92 cm + 14.54 cm + 19.39 cm + 21 cm + 22.62 cm + 24.23 cm + 25.85 cm

Formatted: Font: Times New Roman

Formatted: Font: Times New Roman, Not Italic

Formatted: Right: 0 cm, Tab stops: Not at 1.62 cm + 3.23 cm + 4.85 cm + 6.46 cm + 8.08 cm + 9.69 cm + 11.31 cm + 12.92 cm + 14.54 cm + 19.39 cm + 21 cm + 22.62 cm + 24.23 cm + 25.85 cm

Formatted: Font: Times New Roman

Formatted: Font: Times New Roman

Formatted: Font: Times New Roman, Not Italic

Formatted: Font: Times New Roman

Formatted: Font: Times New Roman, Not Italic

Formatted: Font: Times New Roman

Formatted: Font: Times New Roman, Not Italic

Formatted: Font: Times New Roman

Formatted: Font: Times New Roman, Not Italic

Formatted: Font: Times New Roman

Formatted: Default Paragraph Font, Font: Times New Roman

Field Code Changed

Formatted: Font: Times New Roman

~~Morel, A. and B. Gentili~~, ~~Morel, A., Antoine, D. and B. Gentili, 2002. Bidirectional reflectance of oceanic waters: Accounting for Raman emission and varying particle phase function. Applied Optics, 41, 6289-6306~~

~~Morel, A. and B. Gentili, 2009. A simple band ratio technique to quantify the colored dissolved and detrital organic material from ocean color remotely sensed data, Remote Sensing of Environment, Volume 113, Issue 5, 15 May 2009, Pages 998-1011, ISSN 0034-4257, http://dx.doi.org/10.1016/j.rse.2009.01.008.~~

~~Morel, A. and L. Prieur. Analysis of variations in ocean color. J. Limnology and Oceanography, 22, 709-722, 1977~~

~~NASA Goddard Space Flight Center, Ocean Biology Distributed Active Archive Center; (, 2014); Moderate Resolution Imaging Spectroradiometer (MODIS)-Terra Ocean Color Data, NASA OB.DAAC, Greenbelt, MD, USA. Accessed 09/16/2016. Maintained by NASA Ocean Biology Distributed Active Archive Center (OB.DAAC), Goddard Space Flight Center, Greenbelt MD.~~

NASA Goddard Space Flight Center, Ocean Ecology Laboratory, Ocean Biology Processing Group; (OBPG), 2014; MODIS-Terra L2 chlor_a and l2_flags; NASA Goddard Space Flight Center, Ocean Ecology Laboratory, Ocean Biology Processing Group. Accessed on 09/16/2016.

Sayer, A. M., Thomas, G. E., and Grainger, R. G.; 2010. A sea surface reflectance model for (A)ATSR, and application to aerosol retrievals, Atmos. Meas. Tech., 3, 813-838, doi:10.5194/amt-3-813-2010, 2010.

Sun, J., A. Angal, X-J. Xiong, H. Chen, X. Geng, A. Wu, T-J. Choi, and M. Chu, 2012. MODIS Reflective Solar Bands Calibration Improvements in Collection 6. Proc. of SPIE Vol. 8528, 85280N.

Werdell, P.J. and S.W. Bailey, 2002. The SeaWiFS Bio-optical Archive and Storage System (SeaBASS): Current architecture and implementation, NASA Tech. Memo. 2002-211617, G.S. Fargion and C.R. McClain, Eds., NASA Goddard Space Flight Center, Greenbelt, Maryland MD, 45 pp.

Werdell, P.J. and S.W. Bailey, 2005. An improved in situ data set for bio-optical algorithm development and ocean color satellite validation, Rem. Sens. Environ. 98, 122-140.

Formatted: Right: 0 cm, Tab stops: Not at 1.62 cm + 3.23 cm + 4.85 cm + 6.46 cm + 8.08 cm + 9.69 cm + 11.31 cm + 12.92 cm + 14.54 cm + 19.39 cm + 21 cm + 22.62 cm + 24.23 cm + 25.85 cm

Formatted: Font: Times New Roman

Formatted: Font: Times New Roman

Formatted: Tab stops: Not at 17.62 cm

Formatted: Font: Times New Roman

Formatted: Font: Times New Roman, Not Italic

Formatted: Font: Times New Roman

Formatted: Right: 0 cm, Tab stops: Not at 17.62 cm

Formatted: Font: Times New Roman

Formatted: Font: Times New Roman, Not Italic

Formatted: Font: Times New Roman

|

|

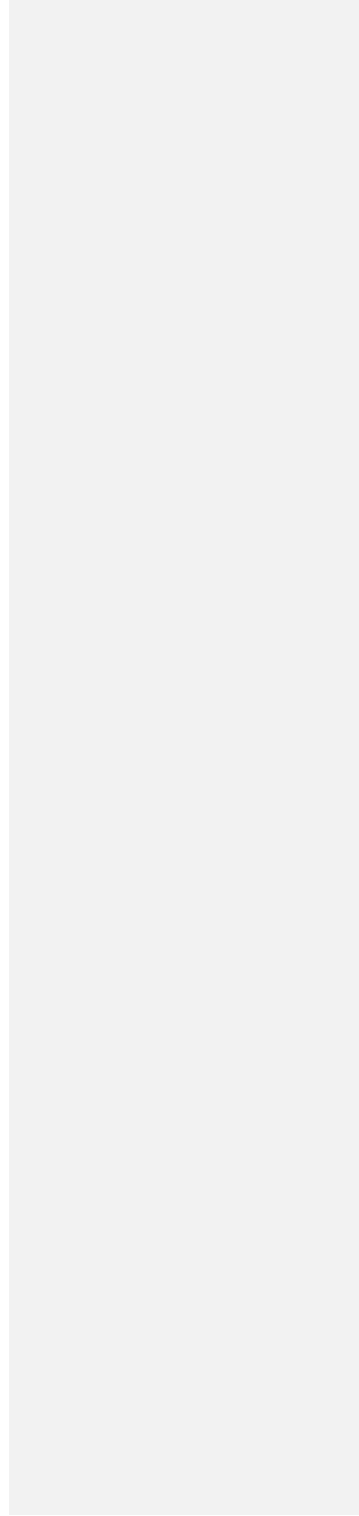


Table 1: Decadal trend values (in percent) aggregated over three stable desert sites for the 36 MISR channels

Fit	Df	Cf	Df	Af	An	An	Dn	Ca	Da
Blue	-1.03	-1.23	-0.85	-1.14	-0.22	-0.44	-0.68	-0.37	-0.20
Green	-1.23	-1.28	-1.21	-1.47	-1.24	-1.12	-1.00	-0.82	-0.63
Red	-1.13	-1.20	-1.23	-1.42	-1.51	-1.24	-1.08	-0.95	-0.80
NIR	-1.15	-1.24	-1.29	-1.46	-1.49	-1.43	-1.29	-1.23	-1.16
95% C.I.#	Df	Cf	Df	Af	An	An	Dn	Ca	Da
Blue	0.20	0.23	0.26	0.20	0.18	0.18	0.22	0.27	0.20
Green	0.28	0.21	0.17	0.15	0.14	0.14	0.16	0.19	0.22
Red	0.17	0.13	0.11	0.09	0.09	0.10	0.11	0.13	0.17
NIR	0.17	0.12	0.10	0.09	0.08	0.09	0.10	0.13	0.21
#	1186	1186	1185	1158	1121	1180	1168	1173	1172

The first four rows present the decadal trends for all 4 MISR wavelengths and 9 cameras. The second four rows represent the 95% Confidence Intervals (CI) for the corresponding trends. The final row gives the number of events for each camera.

Table 2: Statistics of Chlorophyll-a retrievals as compared to SeaBASS

Chl In-situ <1.5	r	MAE	RMSE	Fr. Err	#
<u>Chl_{in situ} <1.5</u>	r	MAE	RMSE	Fr. Err	#
MISR RA	0.86	0.10	0.25	0.52	49
MODIS	0.91	0.14	0.22	0.54	49
MISR RA +vs. MODIS	0.9192	0.10	0.2119	0.4533	49
Chl In- <u>Chl_{in situ} >10.0</u>	r	MAE	RMSE	Fr. Err	#
MISR RA	0.78	0.18	0.37	0.57	75
MODIS	0.88	0.16	0.26	0.52	75
MISR RA +vs. MODIS	0.8690	0.15	0.2922	0.4640	75

In this table, r is the Pearson correlation coefficient, MAE is the median absolute error, RMSE is the root mean squared error between the satellite retrieval and in situ data, Fr. Err is the mean absolute fractional error of the retrieval with respect to the measurement, and # is the number of validation cases included. The last three rows represent row for Chl_{in situ} <1.5 and Chl_{in situ} >10.0 represents the statistics of an averaged MISR/ vs. MODIS retrieval.

|

|

Table 32: Statistics of MISR vs. MODIS Regional Chlorophyll-a retrievals

MISR <i>Chl</i> $\chi^2 < 1.0$, MISR $\chi^2 < 1.0$	r	MAE	RMSE	Fr. Err	#
MODIS <i>Chl</i> < 1.5	0.96	0.09	0.15	0.23	1499610
MODIS <i>Chl</i> < 10	0.94	0.11	0.20	0.29	1829153

In this table, r is the Pearson correlation coefficient, MAE is the median absolute error, RMSE is the root mean squared error between MISR and MODIS-Terra, Fr. Err is the mean absolute fractional error of the MISR RA retrieval with respect to MODIS-Terra, and # is the number of validation cases included.

Formatted: Font: Bold

Formatted: Font: Times New Roman, 9 pt

Formatted: Font: Times New Roman, 9 pt, Italic

Formatted: Font: Times New Roman, 9 pt

Formatted: Font: Times New Roman, 9 pt

Formatted: Font: Times New Roman, 9 pt, Italic

Formatted: Font: Times New Roman, 9 pt

Formatted: Font: Times New Roman, 9 pt

Formatted: Font: Times New Roman, 9 pt, Italic

Formatted: Font: Times New Roman, 9 pt

Formatted: Caption

Table 3: Decadal trend values (in percent) aggregated over three stable desert sites for the 36 MISR channels

<u>Fit</u>	<u>Df</u>	<u>Cf</u>	<u>Bf</u>	<u>Af</u>	<u>An</u>	<u>Aa</u>	<u>Ba</u>	<u>Ca</u>	<u>Da</u>
<u>Blue</u>	<u>-1.03</u>	<u>-1.22</u>	<u>-0.85</u>	<u>-1.14</u>	<u>-0.22</u>	<u>-0.44</u>	<u>-0.68</u>	<u>-0.37</u>	<u>-0.20</u>
<u>Green</u>	<u>-1.22</u>	<u>-1.28</u>	<u>-1.21</u>	<u>-1.47</u>	<u>-1.34</u>	<u>-1.12</u>	<u>-1.00</u>	<u>-0.82</u>	<u>-0.63</u>
<u>Red</u>	<u>-1.13</u>	<u>-1.20</u>	<u>-1.22</u>	<u>-1.42</u>	<u>-1.51</u>	<u>-1.24</u>	<u>-1.08</u>	<u>-0.95</u>	<u>-0.80</u>
<u>NIR</u>	<u>-1.15</u>	<u>-1.24</u>	<u>-1.29</u>	<u>-1.46</u>	<u>-1.49</u>	<u>-1.43</u>	<u>-1.29</u>	<u>-1.22</u>	<u>-1.16</u>
<u>95% CI Fit</u>	<u>Df</u>	<u>Cf</u>	<u>Bf</u>	<u>Af</u>	<u>An</u>	<u>Aa</u>	<u>Ba</u>	<u>Ca</u>	<u>Da</u>
<u>Blue</u>	<u>0.39</u>	<u>0.33</u>	<u>0.26</u>	<u>0.20</u>	<u>0.18</u>	<u>0.18</u>	<u>0.22</u>	<u>0.27</u>	<u>0.29</u>
<u>Green</u>	<u>0.28</u>	<u>0.21</u>	<u>0.17</u>	<u>0.15</u>	<u>0.14</u>	<u>0.14</u>	<u>0.16</u>	<u>0.19</u>	<u>0.22</u>
<u>Red</u>	<u>0.17</u>	<u>0.13</u>	<u>0.11</u>	<u>0.09</u>	<u>0.09</u>	<u>0.10</u>	<u>0.11</u>	<u>0.13</u>	<u>0.17</u>
<u>NIR</u>	<u>0.17</u>	<u>0.12</u>	<u>0.10</u>	<u>0.09</u>	<u>0.08</u>	<u>0.09</u>	<u>0.10</u>	<u>0.13</u>	<u>0.21</u>
<u>#</u>	<u>1186</u>	<u>1186</u>	<u>1185</u>	<u>1158</u>	<u>1131</u>	<u>1180</u>	<u>1168</u>	<u>1173</u>	<u>1172</u>

The first four rows present the decadal trends for all 4 MISR wavelengths and 9 cameras. The second four rows represent the 95% Confidence Intervals (CI) for the corresponding trends. The final row gives the number of events for each camera.

Figure Captions

Formatted: Caption

Formatted: Font: Times New Roman, 9 pt

Formatted: Indent: Left: 0.01 cm

Formatted Table

Formatted: Font: Times New Roman, 9 pt

Formatted: Indent: Left: 0.01 cm

Formatted: Font: Times New Roman, 9 pt

Formatted: Indent: Left: 0.01 cm

Formatted: Font: Times New Roman, 9 pt

Formatted: Indent: Left: 0.01 cm

Formatted: Font: Times New Roman, 9 pt

Formatted: Indent: Left: 0.01 cm

Formatted: Font: Times New Roman, 9 pt

Formatted: Centered, Indent: Left: 0.01 cm

Formatted: Centered

Formatted: Font: Times New Roman, 9 pt

Formatted: Indent: Left: 0.01 cm

Formatted: Font: Times New Roman, 9 pt

Formatted: Indent: Left: 0.01 cm

Formatted: Font: Times New Roman, 9 pt

Formatted: Indent: Left: 0.01 cm

Formatted: Font: Times New Roman, 9 pt

Formatted: Indent: Left: 0.01 cm

Formatted: Font: Times New Roman, 9 pt

Formatted: Indent: Left: 0.01 cm

Formatted: Font: Times New Roman, 9 pt

Formatted: Indent: Left: 0.01 cm

Formatted: Caption

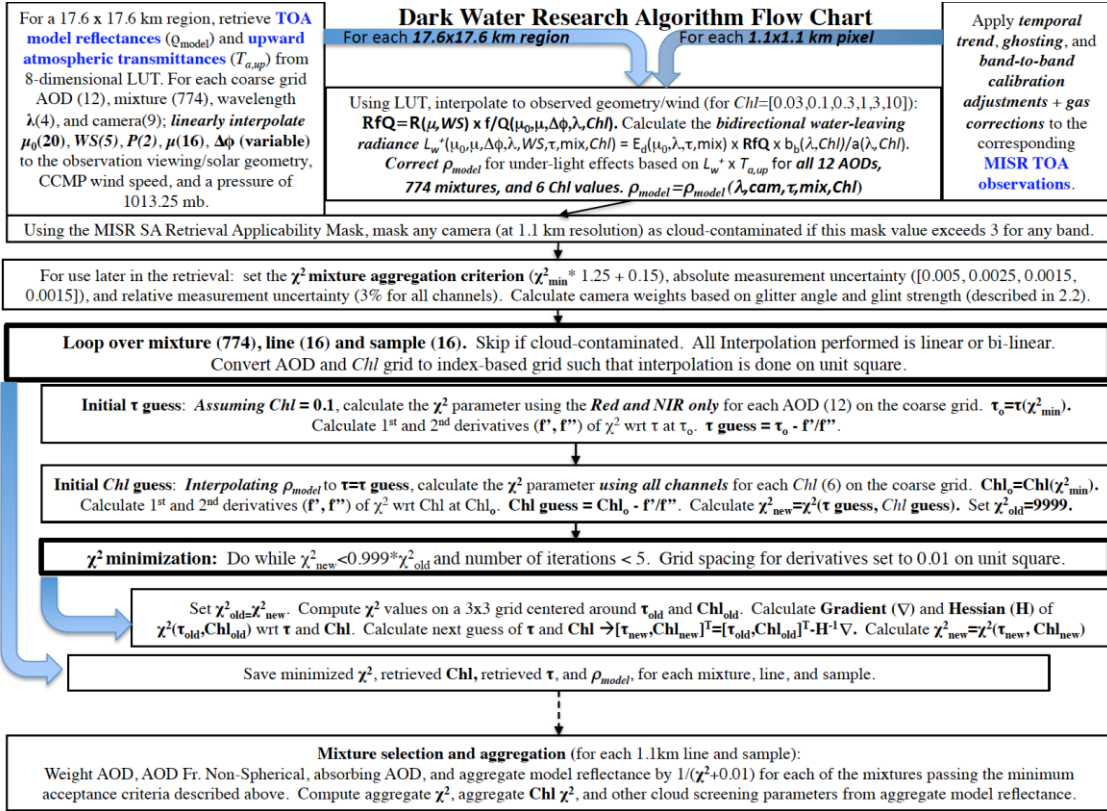


Figure 1

Figure 1. Flow chart describing the MISR RA aerosol/Chl retrieval process.

Formatted: Caption, Right: 0 cm, Tab stops: Not at 16.51 cm

Formatted: Font: 9 pt

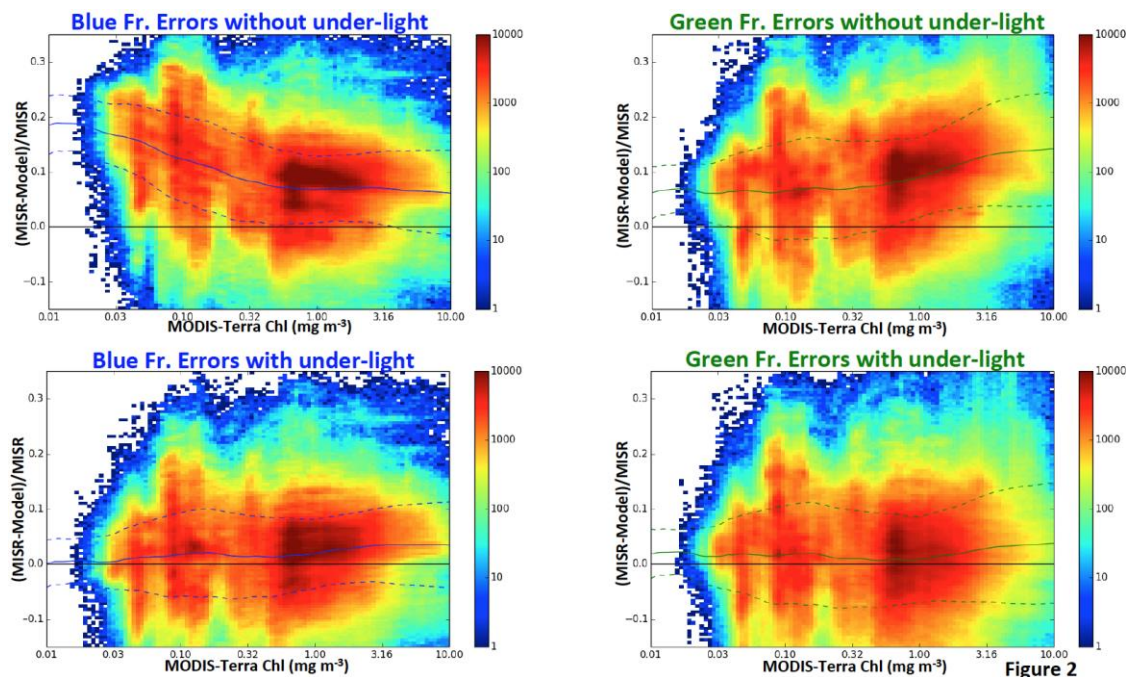


Figure 2. The effect of including under-light, assessed by comparing the MISR-observed TOA reflectances with model-simulated values, not including (top panels) and including (bottom panels) under-light calculated with independently retrieved MODIS *Chl* values. These joint histograms show (MISR - Model)/MISR TOA reflectance for the blue (446 nm, left) and green (558 nm, right) spectral bands, as a function of MODIS *Chl*. All glint-free cameras are aggregated for this analysis. The solid blue (or green) lines represent the smoothed mean bias, and the dashed lines indicate ± 1 smoothed standard deviation. AOD and mixture were obtained by running the RA with under-light included, based on the MODIS *Chl*, and finding the best-fitting mixture and AOD (using only the NIR band, but up to 9 cameras). Once AOD and mixture were obtained, the TOA reflectances were calculated with the forward model, both with and without under-light. Results show that including under-light dramatically lowers the bias in both the blue and green bands for all *Chl* up to 10 mg m^{-3} . As expected, because Chlorophyll-a strongly absorbs in the spectral response range of the MISR blue wavelength, the contribution of under-light to the TOA reflectance decreases with *Chl* in the blue, whilewhereas it increases with *Chl* in the green due to the enhanced scattering from phytoplankton.

Formatted: Font: 9 pt

Formatted: Caption, Right: 0 cm, Tab stops: Not at 5.28 cm

Formatted: Font: Not Bold

Figure 3.

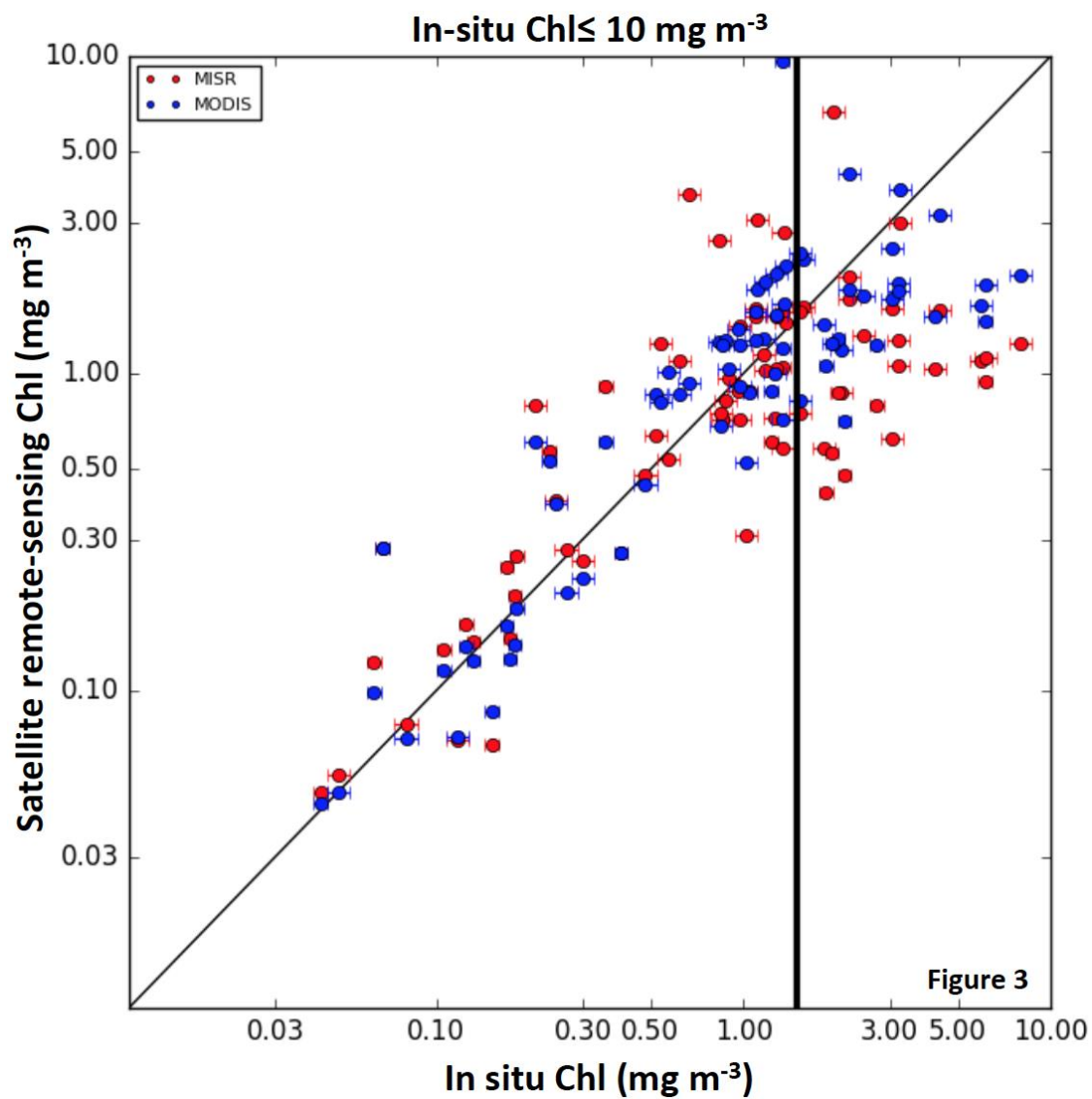


Figure 3. MISR (red points) and MODIS (blue points) remote-sensing Chl (mg m⁻³) versus in situ Chl (mg m⁻³) for Libya 4. Data are normalized such that the mean value of each time series is unity. Dashed black lines indicate ±2 standard deviations. The plots on the left show the MISR AN (nadir camera) data for the four spectral bands, after Step 2d in Section 3 has been performed. The plots on the right show the

Formatted: Caption, Right: 0 cm, Tab stops: Not at 16.51 cm

~~some data after Step 3b is complete. These plots present results for only one of two separate paths covering Libya 4, and for only one of nine cameras. Similar analysis was performed for two paths for each of the three stable desert sites.~~

~~Figure 4. Normalized, de-seasonalized TOA BRF time series plots, for the four spectral bands of the MISR Aa camera. Data are normalized such that the mean value is unity. These data present all of the data for the three desert sites used (Libya 1, Libya 4, and Egypt 1), excluding outliers, processed through Step 4b of Section 3.~~

~~Figure 5. MISR calibration drift per decade (in percent) for all four wavelengths and nine cameras. The data used to generate this plot were aggregated from three pseudo-invariant desert sites (Libya 4, Libya 1, and Egypt 1). The mean decadal trends and the 95% confidence intervals (Student's t test) are plotted.~~

~~Figure 6. MISR (red points), MODIS (blue), and mean MISR/MODIS (green) Chl plotted against SeaBASS validation data for $Chl_{in situ} \leq 10$. Results are presented if both MODIS and MISR have at least one valid retrieval in a 5x5 pixel box surrounding the central SeaBASS location. The vertical black line represents $Chl_{in situ} = 1.5$. We expect better-quality MISR Chl retrievals to the left of this line.~~

Formatted: Font: Not Bold

Formatted: Font: Not Bold

Formatted: Font: Not Bold

Formatted: Caption, Right: 0 cm,
Tab stops: Not at 16.51 cm

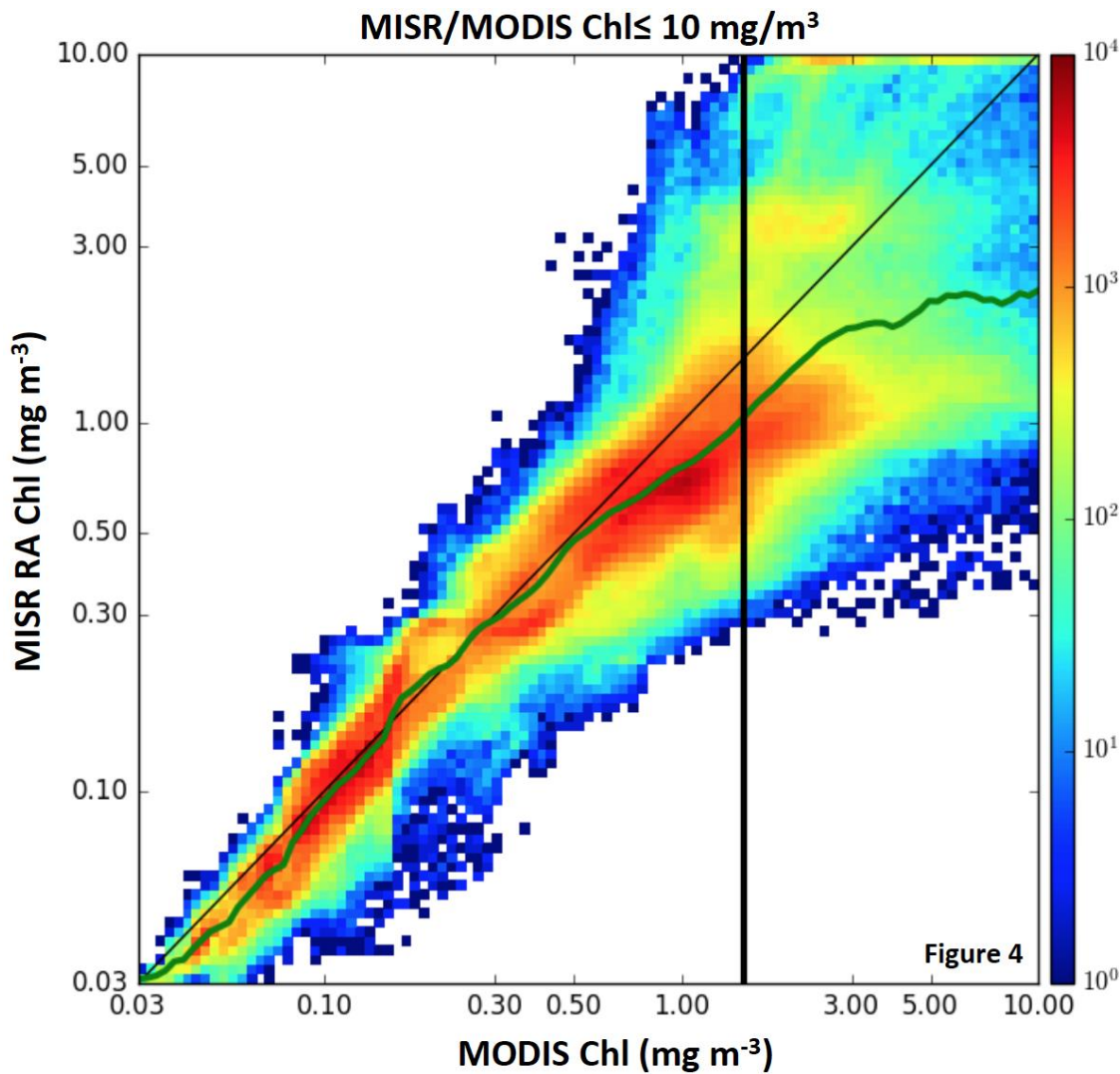


Figure 74. MISR-MODIS *Chl* scatter-density plot for $Chl_{MODIS} \leq 10$. The green line represents the mean MISR *Chl* value for each MODIS *Chl* bin, and the vertical black line represents $Chl_{MODIS} = 1.5$. The bin size used for the green line is roughly 0.03 in \log_{10} space.

Formatted: Right: 0 cm, Tab stops: 5.17 cm, Left + Not at 16.51 cm

Formatted: Font: 9 pt

Formatted: Font: 9 pt

Formatted: Caption, Right: 0 cm, Tab stops: Not at 16.51 cm

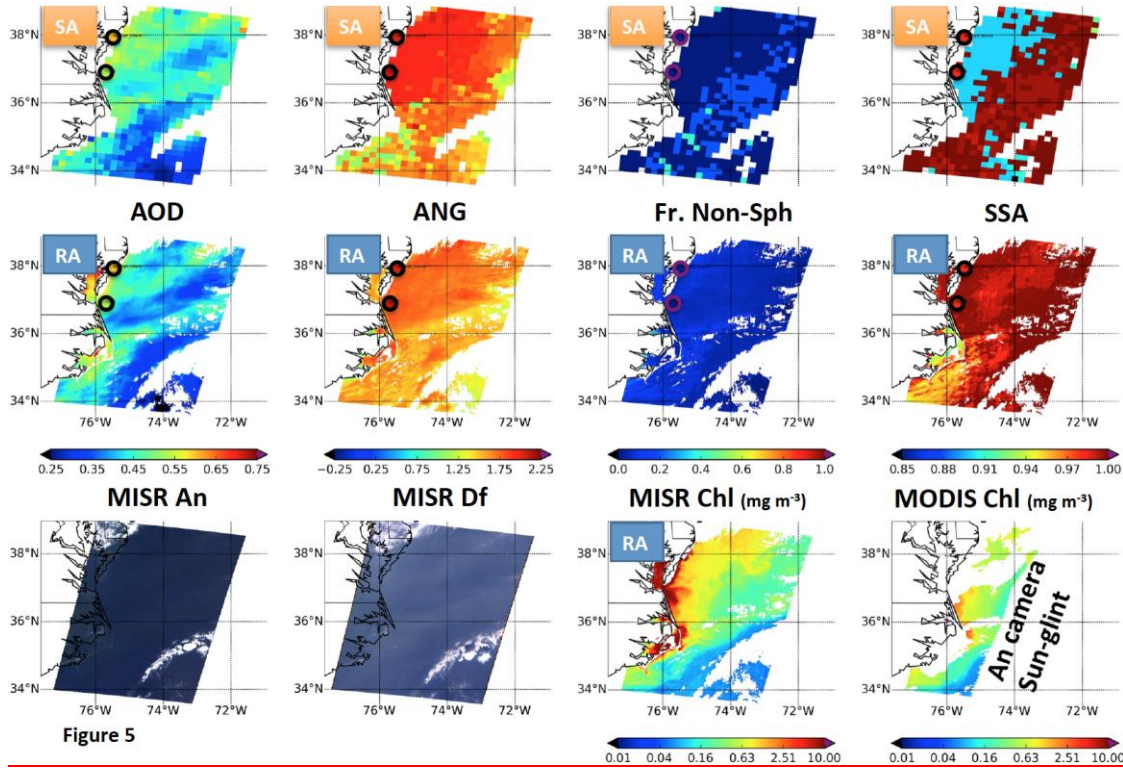


Figure 5

Figure 5. MISR imagery acquired on August 26, 2003, 15:51Z: Terra Orbit 19620, Blocks 60-63, along the US East Coast. Plots compare the MISR SA (at 17.6 km resolution, top row) to the RA that includes retrieved Chl (at 1.1 km resolution, row 2). AOD and particle properties correspond to the MISR green band (558 nm). AERONET direct-sun and inversion values are shown for the COVE and Wallops stations as embedded circles. AERONET Fr. Non-Sph may not be informative when aerosol extinction is dominated by the fine mode. In the lower left, MISR An and Df RGB images are shown for context. MISR-retrieved Chl and MODIS-retrieved Chl are shown in the bottom right two panels.

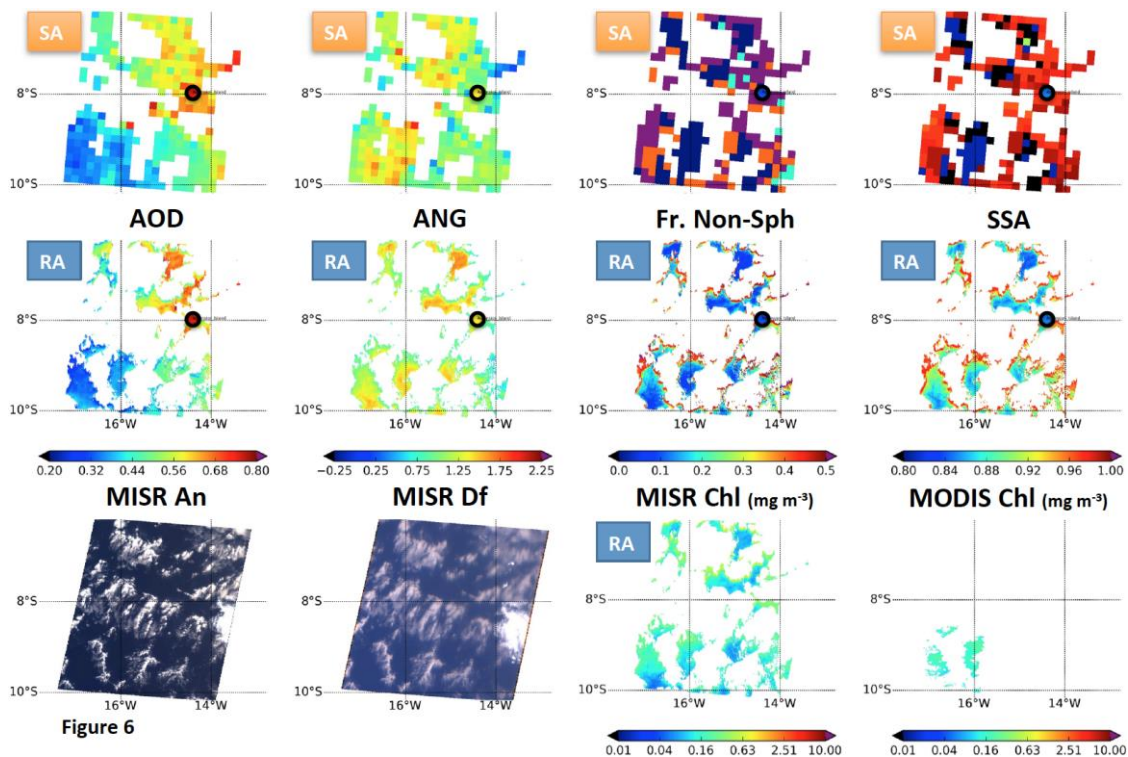


Figure 6. Same as Figure 5, but for data acquired on August 31, 2003, 11:26Z: Terra Orbit 19690, MISR Blocks 96-98, in the mid-south Atlantic Ocean near Ascension Island.

Libya 4 De-seasonalization example:

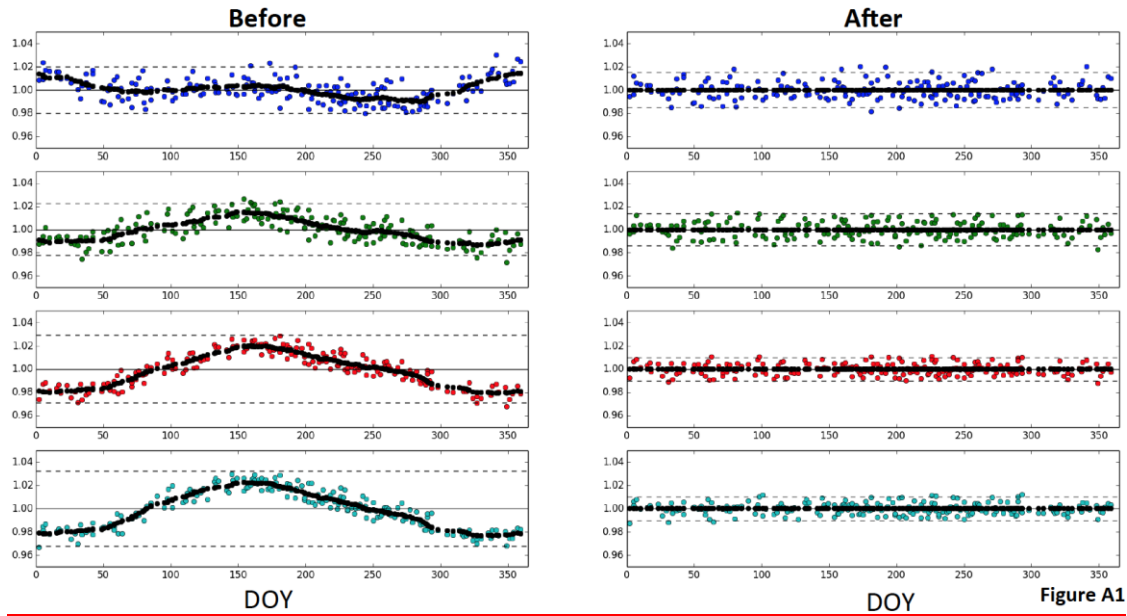


Figure A1

Figure A1. De-seasonalization example for Libya 4. Data are normalized such that the mean value of each time-series is unity. Dashed black lines indicate ± 2 standard deviations. The plots on the left show the MISR An (nadir camera) data for the four spectral bands, after Step 2d in Appendix A has been performed. The plots on the right show the same data after Step 3b is complete. These plots present results for only one of two separate paths covering Libya-4, and for only one of nine cameras. Similar analysis was performed for two paths for each of the three stable desert sites.

Formatted: Caption, Right: 0 cm, Tab stops: Not at 16.51 cm

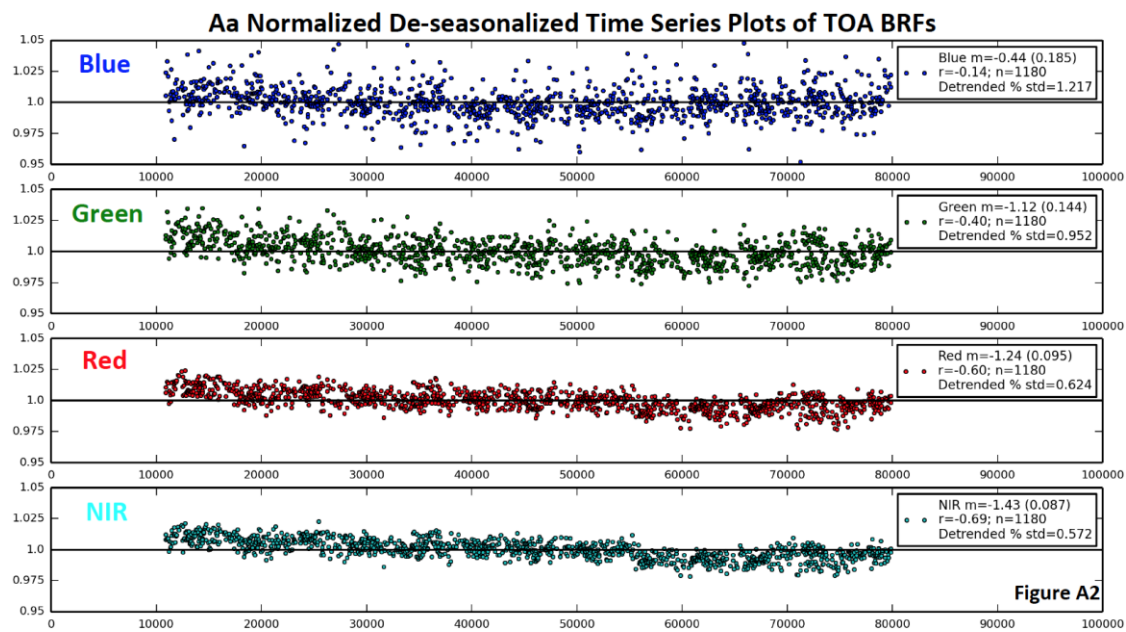


Figure A2. Normalized, de-seasonalized TOA BRF time series plots, for the four spectral bands of the MISR Aa camera. Data are normalized such that the mean value is unity. These data present all of the data for the three desert sites used (Libya-1, Libya-4, and Egypt-1), excluding outliers, processed through Step 4b of Appendix A.

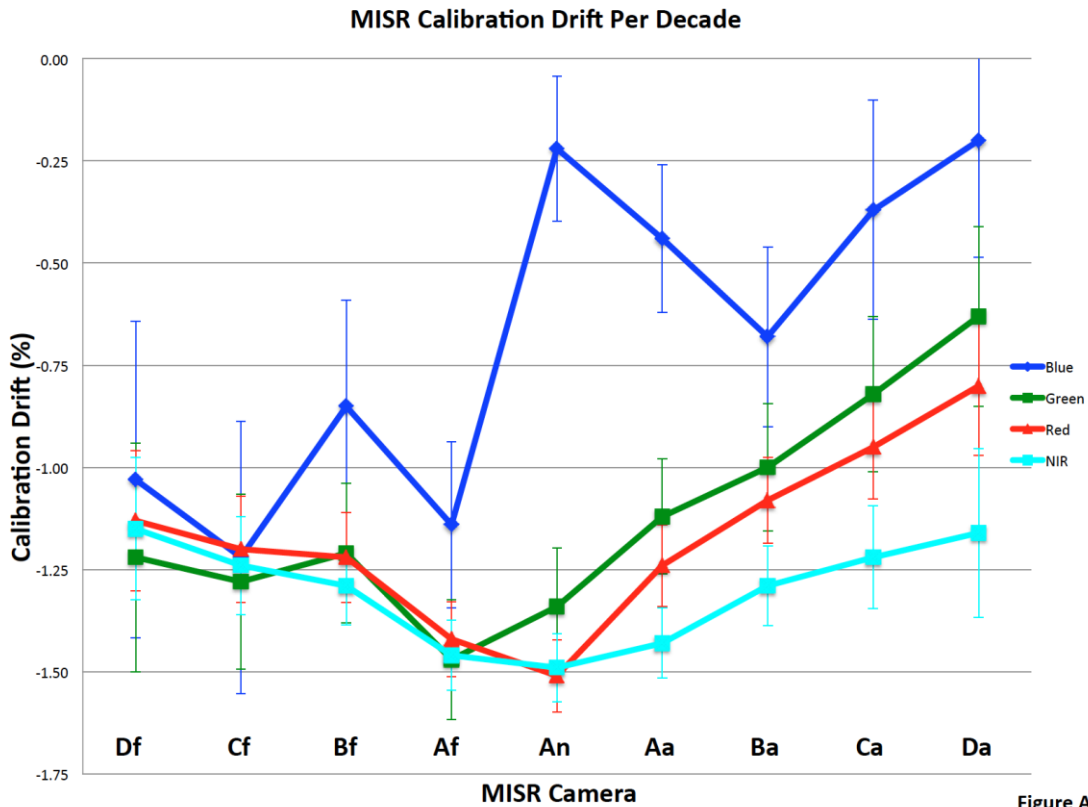


Figure A3

Figure A3. MISR calibration drift per decade (in percent) for all four wavelengths and nine cameras. The data used to generate this plot were aggregated from three pseudo-invariant desert sites (Libya-4, Libya-1, and Egypt-1). The mean decadal trends and the 95% confidence intervals (Student's t-test) are plotted. The viewing angles associated with the MISR cameras are the following (F is forward, A is aft): DF-70.5°, CF-60.0°, BF-45.6°, AF-26.1°, AN-0.0°, AA-26.1°, BA-45.6°, CA-60.0°, DA-70.5°.